Superimposed effects of typical local circulations driven by mountainous topography and aerosol-radiation interaction on heavy haze in the Beijing-Tianjin-Hebei central and southern plains in winter

Yue Peng[1], Hong Wang[1], Xiaoye Zhang[1,2], Zhaodong Liu[1], Wenjie Zhang[1], Siting Li[1], Chen Han[1], Huizheng Che[1]

[1]State Key Laboratory of Severe Weather (LASW) & Key Laboratory of Atmospheric Chemistry of China Meteorological Administration, Chinese Academy of Meteorological Sciences (CAMS), Beijing, 100081, China
[2]Center for Excellence in Regional Atmospheric Environment, IUE, Chinese Academy of Sciences, Xiamen, 361021, China

Correspondence to: Hong Wang (wangh@cma.gov.cn); Xiaoye Zhang (xiaoye@cma.gov.cn)

Abstract. Although China's air quality has substantially improved in recent years due to the vigorous emission reduction, the Beijing-Tianjin-Hebei (BTH) region, especially its central and southern plains at the eastern foot of the Taihang Mountains, has been the most polluted area in China with persistent and severe haze in winter. Combining meteorology-chemistry coupled model simulations and multiple observations, this study explored the causes of several heavy haze events in this area in January 2017, focusing on local circulations related to mountain terrain. The study results showed that on weather scale, the configuration of the upper, middle, and lower atmosphere provided favorable weather and water vapor transport conditions for the development of haze pollution. Under the weak weather-scale systems, local circulation played a dominant role in the regional distribution and extreme values of $PM_{2.5}$. Influenced by the Taihang and Yanshan Mountains, vertical circulations and wind convergence zone were formed between the plain and mountain slopes. The vertical distribution of pollutants strongly depended on the intensity and location of the circulation. The circulation with high intensity and low altitude~~Strong and low circulation~~ was more unfavorable for~~to the~~ vertical and horizontal diffusion~~ and horizontal transport~~ of near-surface pollutants. More importantly, we found that aerosol-radiation interaction (ARI) significantly amplified the impacts of local vertical circulations on heavy haze by two mechanisms. First, ARI strengthened the vertical circulations at the lower levels, with the zonal wind speeds increasing by 0.3~~~2 ~~0.8 $m\ s^{-1}$. Meanwhile, ARI could cause a substantial downward shift of the vertical circulations (~100 m). Second, ARI weakened the horizontal diffusion~~transport~~ of pollutants by reducing the westerly winds ~~below 300 m ~~and enhancing the wind convergence as well as the southerly winds in the polluted area~~below 1000 m~~. Under these two mechanisms, pollutants could only recirculate in a limited space. This superposition of typical local circulation and ARI eventually contributed to the accumulation of pollutants and the consequent deterioration of haze pollution in the region.

1 Introduction

China's air quality has considerably improved in recent years because of aggressive emission reduction measures (Zhang et al., 2019; Zheng et al., 2018). However, the large urban agglomeration such as BTH and the Yangtze River Delta (YRD) still frequently suffer from persistent heavy haze pollution and the deterioration of atmospheric visibility that it causes, especially in winter (Huang et al., 2020; Peng et al., 2020). Particulate matter with an aerodynamic diameter of less than 2.5 μm Fine particulate matter ($PM_{2.5}$) is the primary aerosol component of haze and a significant factor affecting visibility. During heavy haze pollution, $PM_{2.5}$ concentrations often exceeded 300 μg m^{-3}, and sometimes even 500 μg m^{-3} in these areas (Peng et al., 2021; Wang et al., 2018; Zhang et al., 2020). Emissions and meteorological conditions are two key factors affecting pollutants. However, emissions in a region do not change much in the short term, when pollution levels may be dominated by regional or local meteorological conditionsUnder stable emissions, unfavorable meteorological conditions, particularly within the planetary boundary layer (PBL), are closely associated with the cumulative explosive growth of aerosols on haze pollution days (Wang et al., 2018; Zheng et al., 2015; Zhong et al., 2017).

For regional or local air pollution, interactions between ARI, PBL, and long-range transport have been investigated in recent years. ThePrevious studies illustrated that there is a positive feedback between aerosols and the PBL: During heavy haze pollution, high aerosol concentrations weaken the turbulence in the lower troposphere mainly by scattering the solar radiation, thus inhibiting the development of PBL (Miao et al., 2019; Peng et al., 2021; Quan et al., 2013; Wang et al., 2018; Zhong et al., 2018a), while absorbing aerosols, such as black carbon (BC), can heat the upper PBL, and further enhance the stability of the atmospheric stratification (Ding et al., 2016; Huang et al., 2018). The decreased PBL thenassociated with high concentration aerosols increases near-surface relative humidity (RH) by weakening the vertical transport of water vapor; the increased RH in turn promotes the formation of secondary aerosols (Li et al., 2017; Liu et al., 2018). These aerosol direct and semi-direct effects or ARI will eventually deteriorate haze pollution. In addition, aAerosols can also act as cloud condensation nuclei or ice nuclei, modifying cloud physical and radiative properties by participating in cloud microphysical processes, this aerosol-cloud interaction in turn affect the structure and development of the PBL (Zhang et al., 2015; Zhao et al., 2017). Moreover, the PBL feedback can interact with long-range transport through ARI, and this interaction then amplifies transboundary air pollution transport between northern and eastern China (Huang et al., 2020).

In addition to the interactions aboveimpacts of ARI on the PBL meteorology, local circulations driven by unique topography also play an important role in the variations of PBL structure as well as the spatial and temporal distribution of pollutants (Chen et al., 2009; Liu et al., 2009; Miao et al., 2015; Zhang et al., 2018). The BTH region is located in the North China Plain (NCP), with the Yanshan Mountains to the north, Taihang Mountains to the west, and the Bohai Sea to the east (Fig. 1a). The elevation difference between these two mMountains and the NCP can reach 1500–2000 m. Such a complex geographical environment makes the BTH region have unique local atmospheric circulation characteristics and is prone to local accumulation or regional transport of pollutants. Chen et al. (2009) found that the elevation of the pollution layer in Beijing is associated with the mountain-plain breeze, which causes a rapid increase of pollutants in the near-surface in this area. The intensity of local atmospheric circulation can strongly affect the removal and accumulation of local pollutants. In the absence of strong weather systems, the well-developed valley wind circulation and sea breeze circulation over the BTH region are conducive to the long-distance transport of pollutants (Miao et al., 2015). On the contrary, weak local circulations make pollutants recirculate in a limited space and accumulate continuously (Lo et al., 2006; Sun et al., 2013). In addition, several topographic sensitivity experiments have been conducted to examine their effects on the low-level circulation and PBL structure in the BTH (Wang et al., 2019; Zhang et al., 2018), and the results highlight the significance of topography in the formation and accumulation of haze pollution. Despite the fact that there have been numerous previous studies on causes of haze pollution in the BTH, most of them concentrated on the effects of ARI orand topographyic effects aloneseparately, and few studies focused on the link between ARI andwhereas studies on the combined effects of topography-induced local circulation and ARI on pollution (Miao et al., 2020), particularlyand the possible impact of this interaction on haze pollutionthe effects of ARI on local circulation are still scarce.

The BTH suffered several heavy haze episodes between December 2016 and February 2017, with January 2017 being the most representative with persistent and severe pollution. Therefore, focusing on January 2017,Given the key role of the two-way feedback mechanism between aerosol and PBL on heavy pollution accumulation and the dominant role of local circulation on the pollutant distribution under weak weather systems, this study comprehensively investigatedanalyzes the link between local circulation, ARI, and haze in BTH, especially the impacts of ARI on local circulation, using the online coupled atmospheric chemistry model GRAPES_Meso5.1/CUACE.

2 Method and data

2.1 GRAPES_Meso5.1/CUACE and experimental design

GRAPES_Meso5.1/CUACE is an online regional atmospheric chemistry model designed for both operational and research applications. There are two major parts of this model: a weather model GRAPES_Meso5.1 and a chemistry model CUACE. The former is a mesoscale weather prediction model that primarily consists of a fully compressible non-hydrostatical model core and a modularized physics package (Chen et al., 2008); the latter is an online chemistry model that is mainly composed of aerosol and gaseous chemistry modules with emission and dynamic processes (Gong and Zhang, 2008). Wang et al. (2022) established this updated model and provided a comprehensive description of the model. In this model, Peng et al. (2022) implemented the ARI mechanism for the two-way feedback between aerosols and weather processes by incorporating the real-time calculated aerosol optical parameters.

The model domain in this study is centered over the BTH region, covering an area of 33–45 °N in latitude and 110–125 °E in longitude (Fig. 1a). The model has a horizontal resolution of 10 km and 49 unevenly spaced vertical levels ranging from near-surface to 33 km. The physical configuration options selected in this study include the Thompson microphysics (Thompson et al., 2008), the KF cumulus scheme (Kain, 2004), the RRTMG longwave radiation scheme (Mlawer et al., 1997), the Goddard shortwave radiation scheme (Chou et al., 1998) including ARI mechanism, the MRF boundary layer scheme (Hong and Pan, 1996), the MM5 surface layer scheme (Zhang and Anthes, 1982) and Noah land surface scheme (Ek et al., 2003). The chemical configuration options mainly include an emissions inventory treatment system that can process the Multi-resolution Emission Inventory for China (MEIC) of 2017 (Zheng et al., 2018) adopted in this study into the format available for the model, the Second Generation Regional Acid Deposition Model (RADM2) gas-phase chemistry (Stockwell et al., 1990), and the CUACE aerosol model (Gong and Zhang, 2008; Wang et al., 2010, 2015a, 2015b).

2.2 Data

Five categories of data was used in this study: The global Final analysis (FNL) data with a horizontal resolution of 0.25 ° × 0.25 ° (http://rda.ucar.edu/data/ds083.3/) provided by the National Centers for Environmental Prediction (NCEP), which was used for the meteorology initial and lateral boundary fields of the model and the analysis of large-scale circulation in upper and mid-levels; Multi-year climate average of chemical tracers used for chemistry initialization of the model (Wang et al., 2022); Monthly anthropogenic emissions derived from the Multi-resolution Emission Inventory for China (MEIC) of 2017 (Zheng et al., 2018); Hourly near-surface $PM_{2.5}$ mass concentration measured by 149 state-controlled stations provided by the China National Environmental Monitoring Center (http://www.cnemc.cn/) and 210 stations provided by the Hebei Meteorological service; Vertical meteorology data for three sounding stations in BTH, i.e., Beijing (BJ), Tangshan (TS), and Xingtai (XT), including air pressure, temperature, and wind at 08:00 and 20:00 Beijing time (BJT) each day, measured by the L-band radiosonde system.

2.3 Experimental design and data analysis method

The model simulation was conducted from December 29, 2016, to January 31, 2017, with a looping time of 72 h. The first 72 h simulations were considered the spin-up period. To evaluate the impacts of ARI on $PM_{2.5}$ concentration, two numerical scenarios were performed in this study. The first is the controlling simulation (CTL) with the above model configurations and ARI; the second is the sensitive experiment (EXP) which is consistent with CTL but without consideringdoes not consider ARI. The same analysis data and emission inventory were used for both numerical scenarios.

Multiple model performance evaluation metrics were used, including the correlation coefficient (r), the mean bias (MB), the root mean square error (RMSE), the mean fractional bias (MFB), and the mean fractional error (MFE). The equations of these metrics are available in Boylan and Russell (2006).

2.2 Data

Four categories of data was used in this study: The global Final analysis (FNL) data with a horizontal resolution of 0.25 ° × 0.25 ° (http://rda.ucar.edu/data/ds083.3/) provided by the National Centers for Environmental Prediction (NCEP), which was used for the meteorology initial and lateral boundary fields of the model and the analysis of large-scale circulation in upper and middle levels; Multi-year climate average of chemical tracers used for chemistry initialization of the model (Wang et al., 2022); Hourly near-surface $PM_{2.5}$ mass concentration measured by 149 state-controlled stations provided by the China

National Environmental Monitoring Center (http://www.cnemc.cn/) and 210 stations provided by the Hebei Meteorological service; Vertical meteorology data for three sounding stations in BTH, i.e., Beijing (BJ), Tangshan (TS), and Xingtai (XT), including air pressure, temperature, and wind at 08:00 and 20:00 Beijing time (BJT) each day, measured by the L-band radiosonde system.

3 Results and discussion

3.1 Model performance

Accurate reproduction of aerosol concentration variations and the vertical structure of the atmosphere is a prerequisite for quantifying ARI (Zhang et al., 2015) as well as local circulation. Figure 1 shows the distribution of observed and simulated monthly mean $PM_{2.5}$ concentrations in January 2017. The BTH region suffered from severe haze pollution in January 2017, with its regional monthly mean observed $PM_{2.5}$ concentration reaching 130 μg m^{-3}. Particularly at the eastern foot of the Taihang Mountains, the central and southern plains of BTH, the $PM_{2.5}$ values exceeded 200 μg $m^{-3}$and even 250 μg m^{-3}. High anthropogenic emission coupled with a stable atmosphere due to the mountainous topography leads to frequent and severe haze events in this area (Fu et al., 2014). BTH is surrounded by the Yanshan and Taihang Mountains from north to west, and such topography is not conducive to pollutant dispersion since the mountains weaken the cold air from the north and west and block the transport of pollutants associated with easterly and southerly winds (Gao et al., 2017; Miao et al., 2015; Quan et al., 2020; Zhong et al., 2018b). The comparison of the observed and simulated $PM_{2.5}$ results (Fig. 1c–d) shows that although both simulation scenarios reproduced the distribution of $PM_{2.5}$ concentrations, the CTL results with ARI were closer to the observations. For the whole BTH region, the mean biases of the simulated results for CTL and EXP were -17 and -41 μg m^{-3} , respectively. Particular inFor the most polluted central and southern BTH, the maximum $PM_{2.5}$ concentration exceeded 225 μg m^{-3} in CTL andwhile was less than 200 μg m^{-3} in EXP. This result not only demonstrates the applicability of the model, but also the need to consider ARI effects for pollutant simulation.

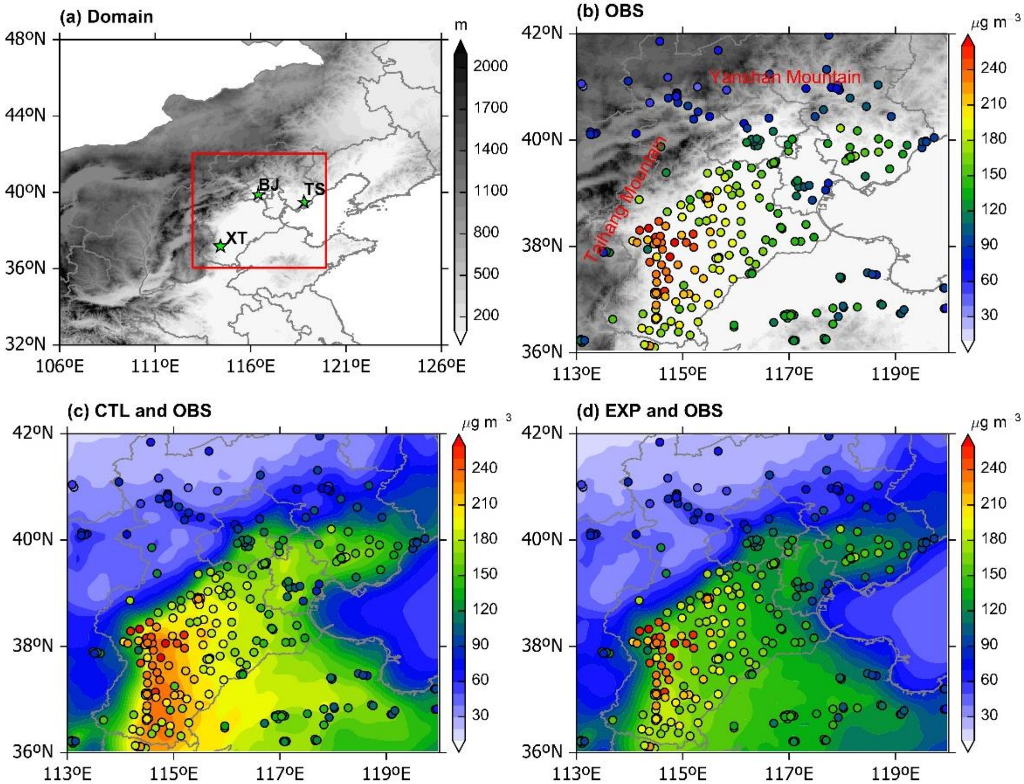
(a) Domain
(b) OBS
(c) CTL and OBS
(d) EXP and OBS
Yanshan Mountain
Taihang Mountain
BJ
TS
XT
m
μg m⁻³
48ºN
44ºN
40ºN
36ºN
32ºN
106ºE
111ºE
116ºE
121ºE
126ºE
42ºN
38ºN
113ºE
115ºE
117ºE
119ºE
2000
1700
1400
1100
800
500
200
240
210
180
150
120
90
60
30

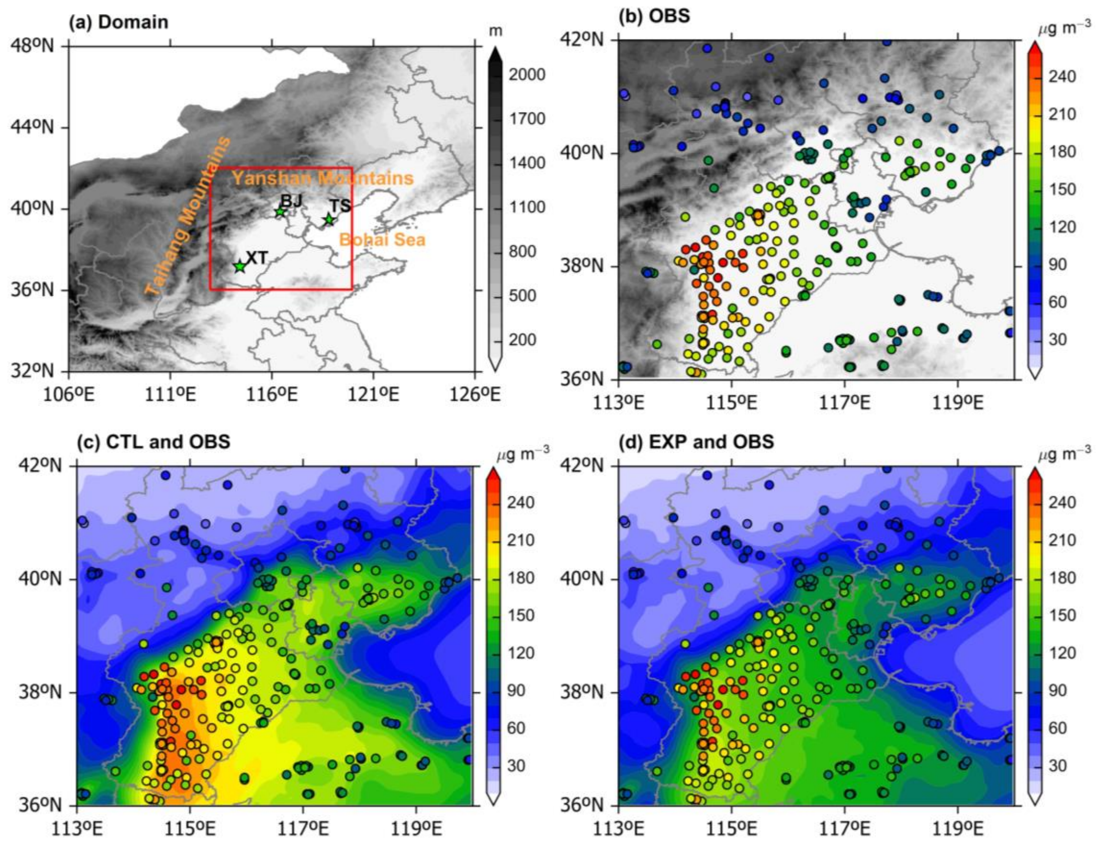

Figure 1. (a) Model domain (shading denotes terrain height; red rectangle shows the general location of BTH; green start denotes the weather sounding station) and (b–d) spatial distributions of observed (OBS: circles) and simulated (CTL and EXP: shadings) $PM_{2.5}$ concentrations in January 2017.

The hourly variation of observed and simulated $PM_{2.5}$ concentrations in BTH was compared in Fig. 2. The model generally reproduced the temporal variation of observed $PM_{2.5}$~~;~~. ~~with correlation coefficients of 0.74 and 0.71 for CTL and EXP, respectively. This result also demonstrated that the simulations of CTL were more consistent with observations, which significantly improved the underestimation of high~~ ~~$PM_{2.5}$~~ ~~concentrations through the ARI mechanism.~~ Compared to EXP, the model including ARI (CTL) showed better agreements with observations, with higher r (from 0.71 to 0.74), smaller MB (from -40.2 to -16.4 μg m^{-3}), and smaller RMSE (from 57.0 to 45.3 μg m^{-3}) (Table 1). Besides, both MFB and MFE showed substantial reductions, from -34.2 μg m^{-3} and 37.6 μg m^{-3} to -15.7 μg m^{-3} and 28.5 μg m^{-3}, respectively (Table 1). According to model performance goals for $PM_{2.5}$ proposed by Morris (2005), both CTL and EXP simulation results achieved an average level (MFB ≤ ±60% and MFE ≤ 75%), with CTL exceeding a good level (MFB ≤ ±30% and MFE ≤ 50%) and very close to an excellent level (MFB ≤ ±15% and MFE ≤35%). The result not only demonstrates the applicability of the model, but also the necessity of considering ARI for pollutant simulation. Moreover, the ARI effect strongly depends on the $PM_{2.5}$ concentrations (Peng et al., 2021; Zhang et al., 2022). In this study, the ARI effect was significant when the $PM_{2.5}$ concentration was larger than 100 μg m^{-3} (Fig. 2), implying that the ARI effect can significantly improve the model's underestimation of the $PM_{2.5}$ peaks. ConsideringGiven the essential influence of that the ARI mechanismshort-term characteristics of the local circulation have a greater influence on the $PM_{2.5}$ extremes values of $PM_{2.5}$ than its long-term characteristics, and the accuracy of the simulation results, representative pollution days will be selected for this study. three pollution periods were selected: As shown in Fig. 2, the BTH region suffered from several persistent heavy haze pollutions throughout the month, and the daily mean $PM_{2.5}$ concentrations kept climbing upward and exceeded 100 μg m^{-3} on January 15–7, 16–18, and 23–26. Furthermore, since the short-term characteristics of the local circulation have a greater impact on the $PM_{2.5}$ distribution than the long-term, it is necessary to select one day from each of the three periods to further investigate the link between local circulation and ARI and how their processes enhance heavy haze pollution. According to the criteria of air pollution level (HJ633–2012) issued by the Ministry of Environmental Protection of China, heavy pollution is defined as the daily mean PM_{25} concentration larger than 150 μg m^{-3}. Therefore, we finally selected January 6, 17, and 2425, which reached the heavy pollution level and were in the rising stage, were finally selected as the representatives of heavy pollution days in three pollution periods., considering the simulation results and $PM_{2.5}$ concentrations.

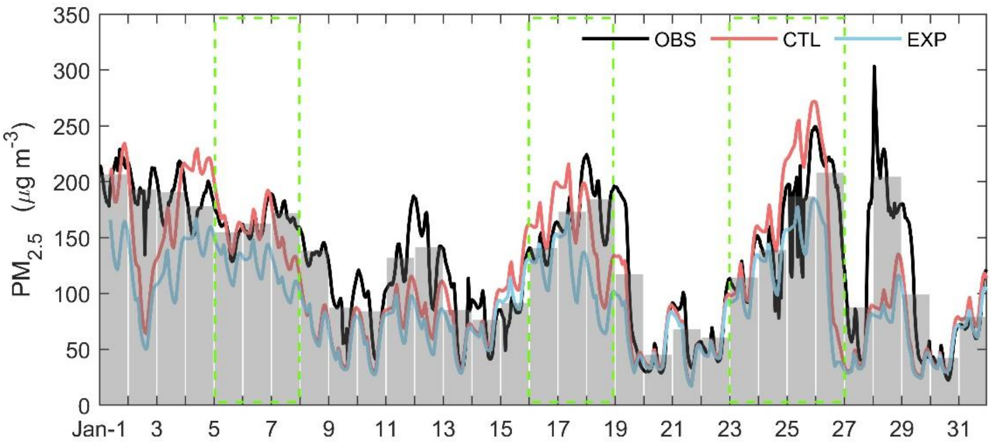

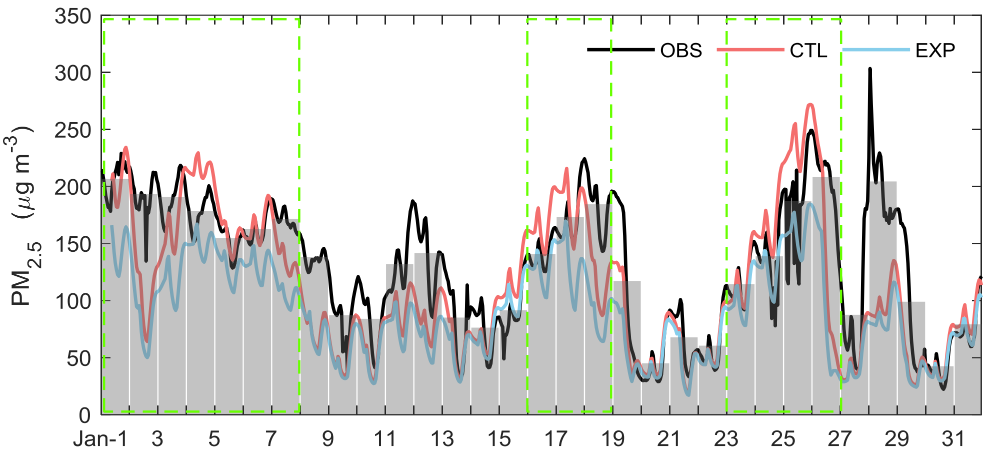

Figure 2. Time series of observed (OBS) and simulated (CTL and EXP) $PM_{2.5}$ concentrations in BTH during January 2017. Grey bar: observed daily mean $PM_{2.5}$ concentrations; Green box: selected pollution period.

Table 1. Model evaluation for $PM_{2.5}$ in BTH during January 2017.

	r	MB $\mu g\ m^{-3}$	RMSE $\mu g\ m^{-3}$	MFB %	MFE %
CTL	0.74	-16.4	45.3	-15.7	28.5
EXP	0.71	-40.2	57.0	-34.2	37.6

Given the important influence of atmospheric vertical structure, especially temperature stratification, on the formation of pollutants, we further evaluated the model performance (CTL) in simulating the vertical profile of the potential temperature (PT) at BJ, TS, and XT by comparing sounding observations. As shown in Fig. 3, the model simulations reasonably reproduced the vertical distribution of temperature in BJ, TS, and XT, including a good simulation of atmospheric warming during the pollution period. For the three pollution periods (January 1–7, 16–18, and 23–26), the mean values of r for PT below 2500 m were 0.94, 0.97, and 0.97 in BJ, TS, and XT, respectively; for the ~~selected~~ heavy pollution days (January 6, 17, and 25~~4~~), the r values ~~correlation coefficients of PT below 2500 m~~ were 0.83~~~–~~0.99 in BJ, 0.96~~~–~~0.99 in TS, and 0.90~~~–~~0.99 in XT. The accurate representation of near-surface $PM_{2.5}$ concentrations and vertical temperature structure in the model provides a solid basis for clarifying the physical mechanisms of heavy pollution.

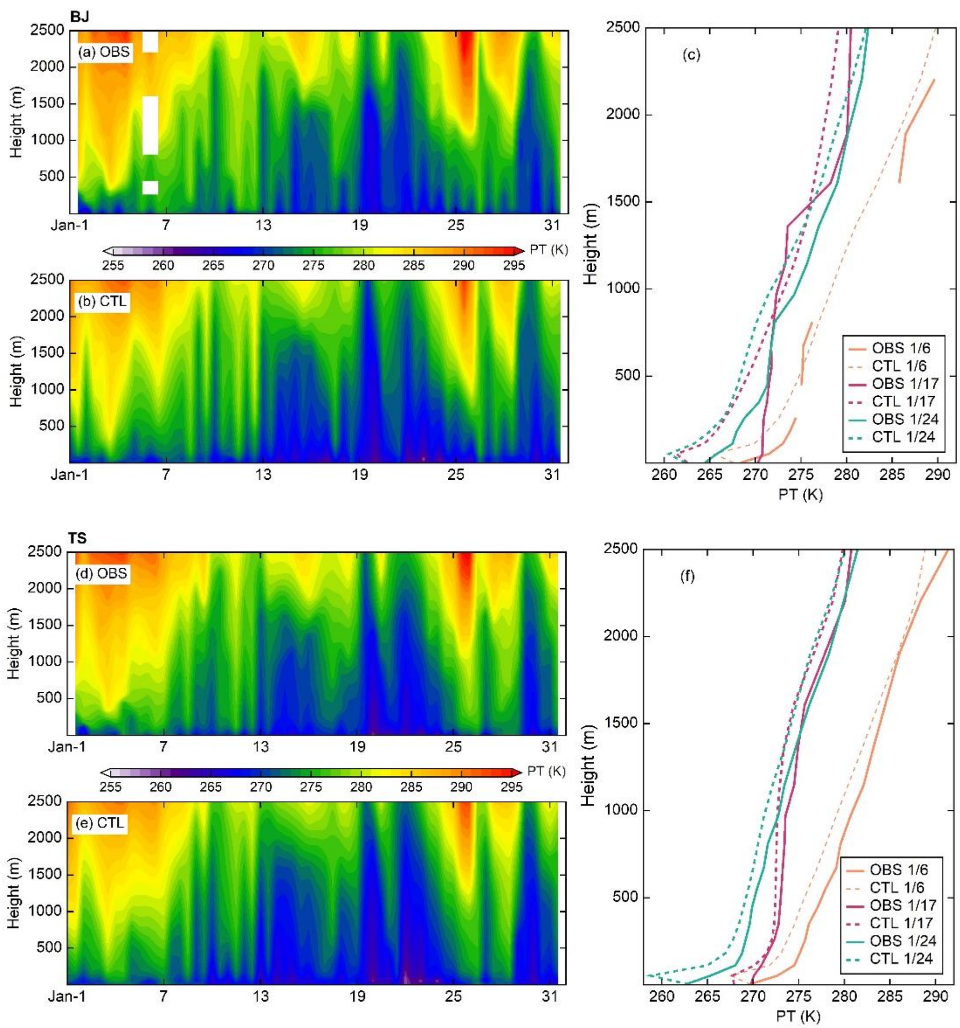

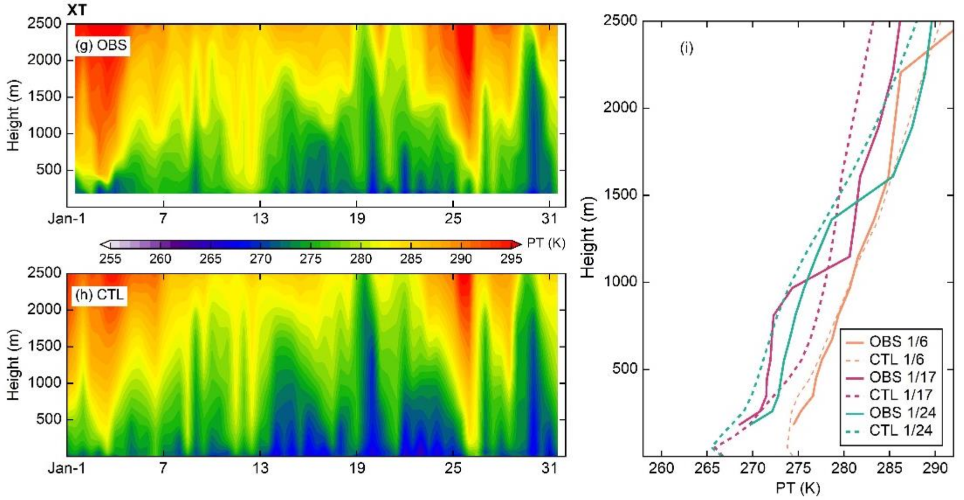
XT
(g) OBS
(h) CTL
(i)
Height (m)
PT (K)
Jan-1
7
13
19
25
31
255
260
265
270
275
280
285
290
295
OBS 1/6
CTL 1/6
OBS 1/17
CTL 1/17
OBS 1/24
CTL 1/24

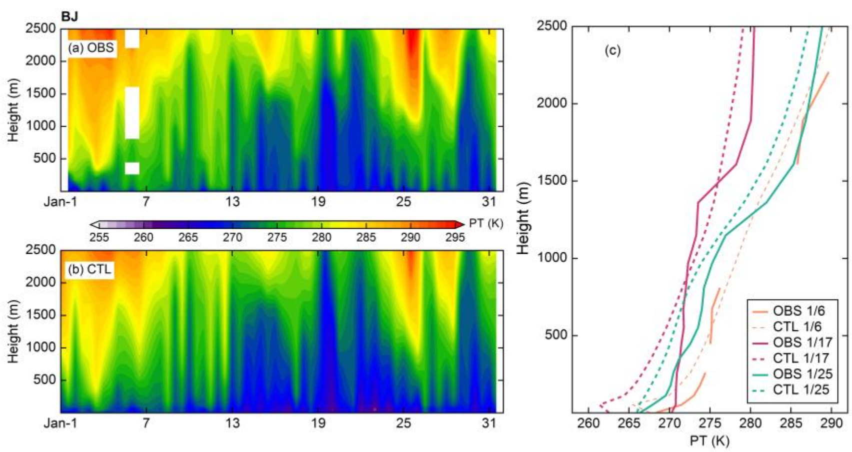
BJ
(a) OBS
(b) CTL
(c)
Height (m)
PT (K)
Jan-1
7
13
19
25
31
OBS 1/6
CTL 1/6
OBS 1/17
CTL 1/17
OBS 1/25
CTL 1/25

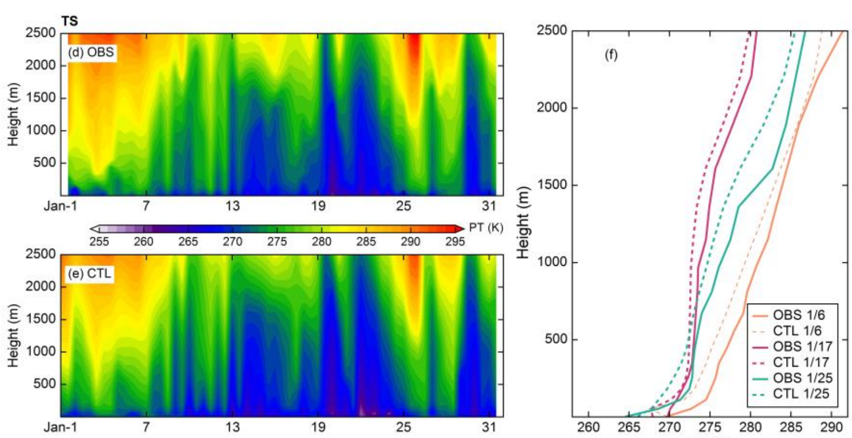
TS
(d) OBS
(e) CTL
(f)
Height (m)
PT (K)
Jan-1
7
13
19
25
31
OBS 1/6
CTL 1/6
OBS 1/17
CTL 1/17
OBS 1/25
CTL 1/25

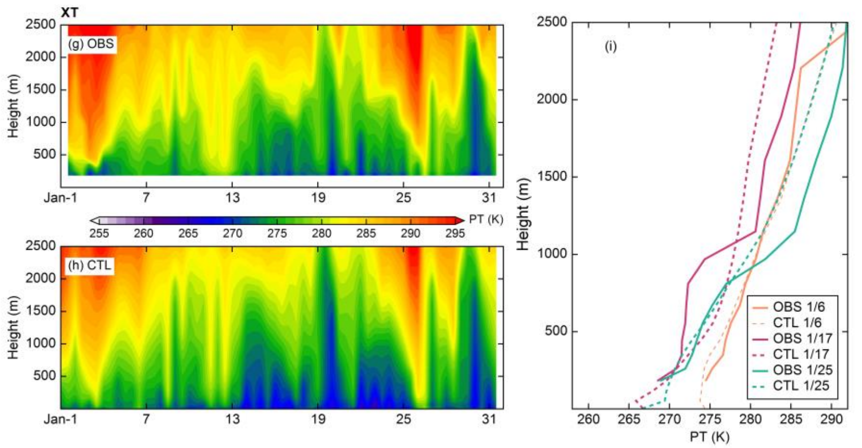

Figure 3. Vertical profiles of observed (OBS) and simulated (CTL) PT for (a–b) BJ, (d–e) TS, and (g–h) XT at 08:00 and 20:00 BJT in January 2017. c, f, and i denote the PT profiles for these three cities at 08:00 BJT on January 6, 17, and 25~~4~~.

3.2 Weather situation background under haze pollution

Previous studies have shown that persistent pollution is influenced not only by the PBL and surface meteorology but also by the configuration of upper and lower-level circulation systems (Miao et al., 2015; Wu et al., 2017). Based on the distribution characteristics of pollutants in the BTH region and the good simulation performance of the model, the horizontal distribution of the upper, middle, lower atmosphere and surface circulation field in the pollution days was examined in this section. ~~First~~Before the specific discussion of the three heavy haze days, we made a general analysis of the weather situation in the three pollution periods. Fig. S1 (in the Supplement) shows the average distributions of geopotential height (GH), PT, and wind vectors at the 500 and 700 hPa levels ~~on January 6, 17, and 24 were discussed using~~from the FNL data. It can be seen that the BTH region was basically controlled by northwesterly airflow at upper and mid-levels during the pollution periods, and its PT increased with height. This is a typical atmospheric circulation that often accompanies pollution episodes.~~Previous studies have shown that persistent pollution is influenced not only by the PBL and surface meteorology but also by the configuration of upper and low-level circulation systems (Miao et al., 2015; Wu et al., 2017).~~ The distributions of simulated (CTL) GH and PT at 850 hPa were similar to those at 500 and 700 hPa (Fig. S2). The BTH region was dominated by a uniform pressure field in front of the high pressure system. The weak pressure gradient resulted in weak westerly wind flows, which blocked dry and cold polar air into this region. Under the stable atmospheric circulation conditions, the PBL development over BTH was suppressed, which led to lower height of the PBL (PBLH) and near-surface wind speeds, contributing to the formation and maintenance of haze pollution (Fig. S3).

Based on the above results, we further compared the weather situation characteristics of the selected heavy pollution day in each period. The circulation patterns across the BTH differed considerably during these three days (Fig. 4). On January 6, eastern China was in front of a weak north-south trough at 500 hPa, and the BTH region was controlled by southwest airflow and a slight temperature gradient. On January 17, a zonal circulation dominated East Asia, and a zonal westerly airflow was in charge of the BTH region. On January 25~~4~~, mainland China was dominated by a northeast-southwest high pressure ridge, and the BTH region was controlled by westerly and northwesterly airflow over~~in front of~~ this ridge. Moreover, the circulation patterns at 700 hPa were consistent with that at 500 hPa. All these synoptic conditions are generally considered to promote the deterioration of pollution since they impede the southward movement of cold air from the north and west and strengthen the downdraft (Wu et al., 2017; Zhang et al., 2019).

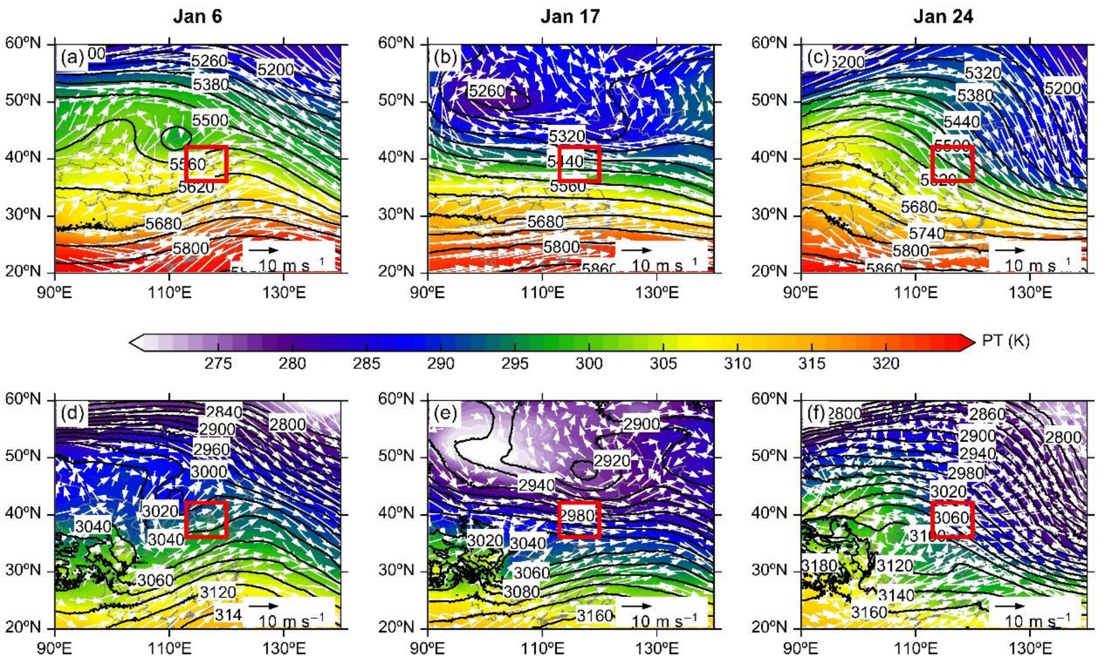

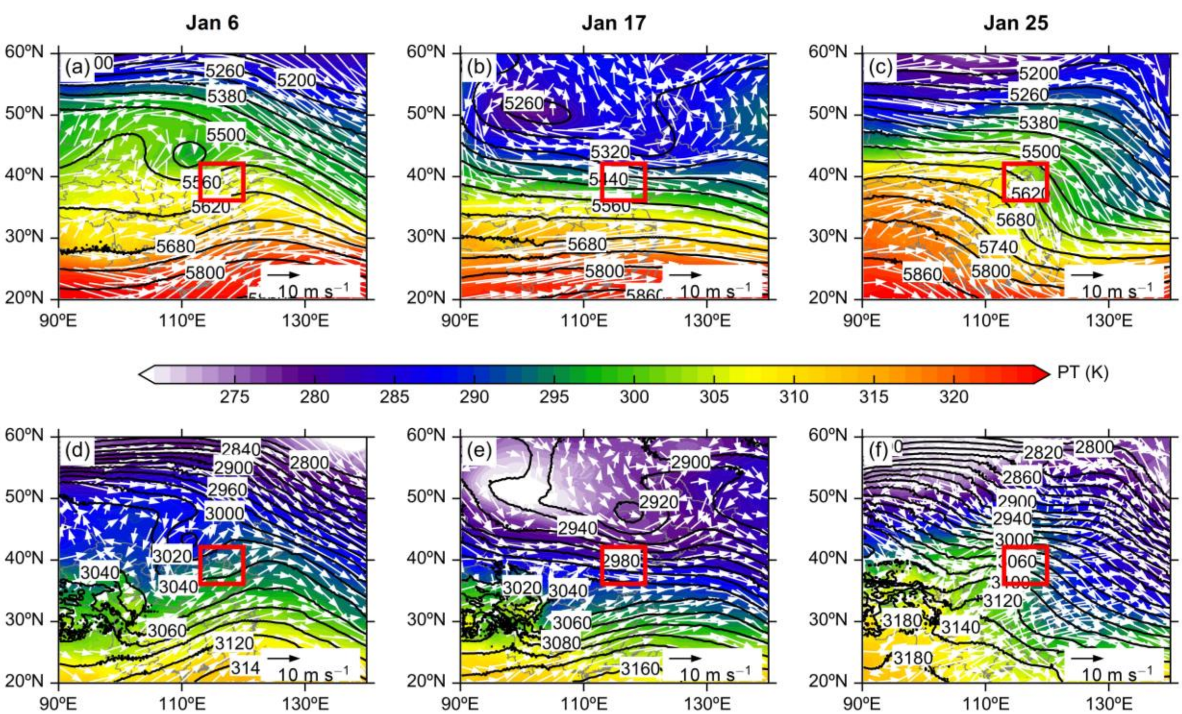

Figure 4. Distribution of GH (black line), PT (shading), and wind vectors (white arrow) at (a–c) 500 and (d–f) 700 hPa on January 6, 17, and 254. Red rectangles indicate the BTH region.

Figure 5 displays the distribution of simulated GH, PT, and wind vectors at 850 hPa level on the three days. On January 6, most of the BTH region was between two weak high pressures. Influenced by the southwesterly and southeasterly winds, the warm and humid air masses from the south and the sea were brought to the central and southern BTH. The northern BTH was mainly controlled by low pressure to the northeast, and the northwesterly winds in the area were reduced due to the blockage of the Taihang and Yanshan Mountains. On January 17, the BTH region was between the low pressure in the northeast and the high pressure in the southwest, leaving most of BTH under the control of northwesterly winds. On January 25~~4~~, eastern China was under the control of subtropical high pressure. The BTH region was located north of the subtropical high center, with ~~westerly and~~ southwesterly winds prevailing. ~~At the same time, 850 hPa temperature decreased from southwest to northeast, and s~~Such a wind field is ~~also~~ conducive to bringing ~~the~~ warm and humid air masses from the south to BTH.

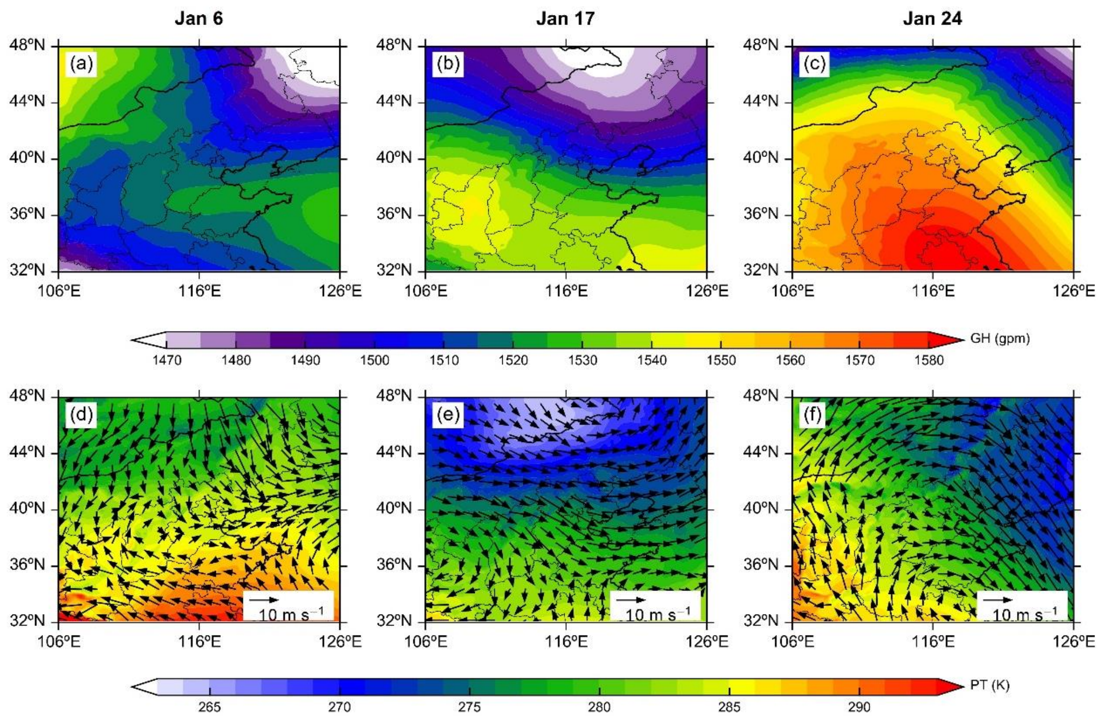
Jan 6
Jan 17
Jan 24
(a)
(b)
(c)
(d)
(e)
(f)
48ºN
44ºN
40ºN
36ºN
32ºN
106ºE
116ºE
126ºE
GH (gpm)
1470 1480 1490 1500 1510 1520 1530 1540 1550 1560 1570 1580
10 m s⁻¹
PT (K)
265 270 275 280 285 290

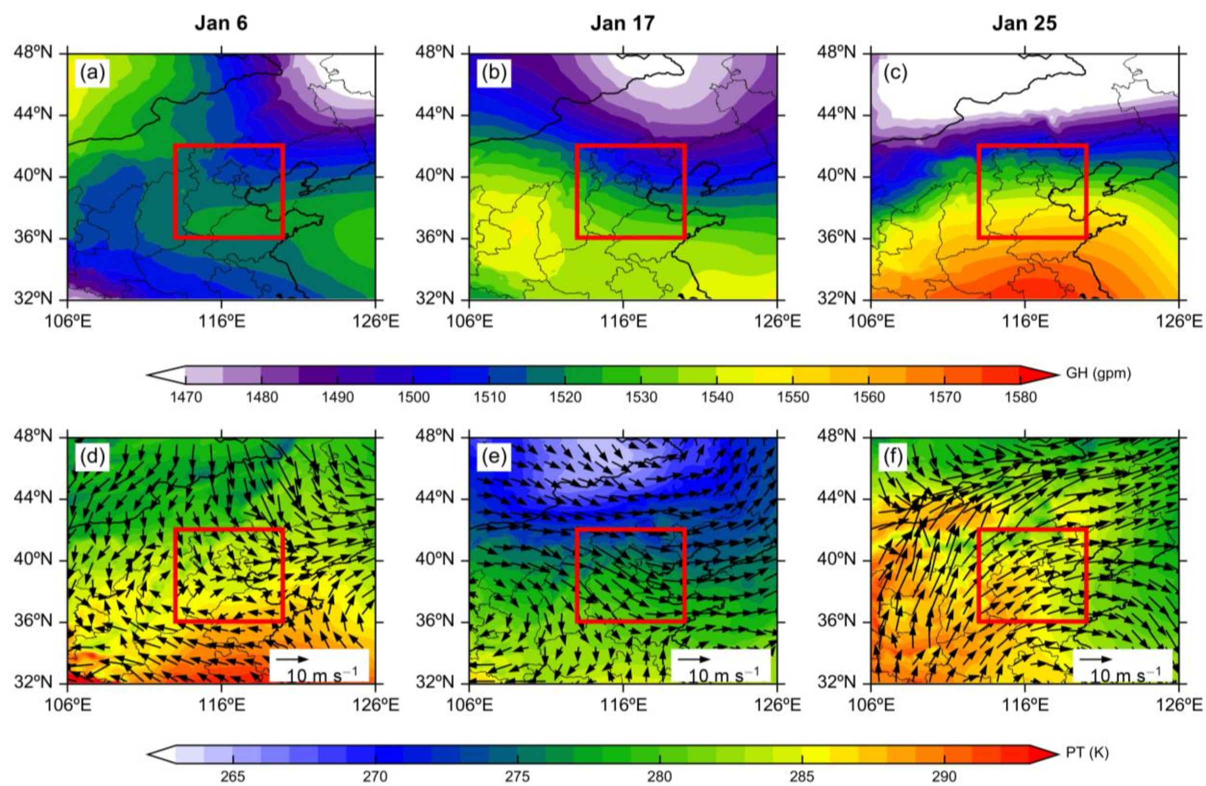
Jan 6
Jan 17
Jan 25
(a)
(b)
(c)
(d)
(e)
(f)
48ºN
44ºN
40ºN
36ºN
32ºN
106ºE
116ºE
126ºE
GH (gpm)
1470 1480 1490 1500 1510 1520 1530 1540 1550 1560 1570 1580
10 m s⁻¹
PT (K)
265 270 275 280 285 290

Figure 5. Distribution of simulated (CTL) GH (a–c), PT (d–f: shading), and wind vectors (d–f: black arrow) at 850 hPa on January 6, 17, and 25~~4~~. Red rectangles indicate the BTH region.

The northerly or northwesterly airflow in the lower troposphere tends to form a sink motion on the leeward slope after being blocked by the Yanshan and Taihang Mountains, which will lead to a decrease in ~~the height of the~~ PBLH ~~(PBLH)~~ and ~~the~~ wind speed in the plains of BTH region (Fig. 6). On the three days, the daily mean PBLH was generally below 300 m in the central and southern plains of BTH, and its low-value area corresponded well to the high-value area of near-surface $PM_{2.5}$ concentrations. Moreover, due to the disturbance of local circulation caused by the Yanshan and Taihang Mountains, the near-surface wind field showed different distribution characteristics from the lower troposphere with wind speeds below 2 $m\ s^{-1}$ in most areas. On January 6, high $PM_{2.5}$ concentrations were concentrated in eastern BTH, and a northeast-southwest transport channel was formed under the influence of northeasterly winds. This distribution of wind filed was consistent with the average result during the three pollution periods (Fig. S3b). On January 17, northwesterly winds prevailed in the northern Beijing area due to strong airflow in the lower troposphere. However, the blockage of the mountains made the airflow sharply weakened in the plain area after crossing the mountains, and formed subsidence and weak divergence, which led to a large accumulation of pollutants here. A similar transport channel was found on January 25, while its wind field was completely different from that on January 6. Most of the plains are controlled by southerly winds. The southerly winds formed a convergence zone with the northerly winds south of Beijing, which was not conducive to the outward dispersion of pollutants. Furthermore, the southerly winds brought warm and humid air mass from the south, which facilitated the formation of secondary pollution.~~The distribution of wind fields in the plain of BTH on January 24 was similar to that on January 6, and there was also a pollution transport channel from southern Beijing to Xingtai area.~~

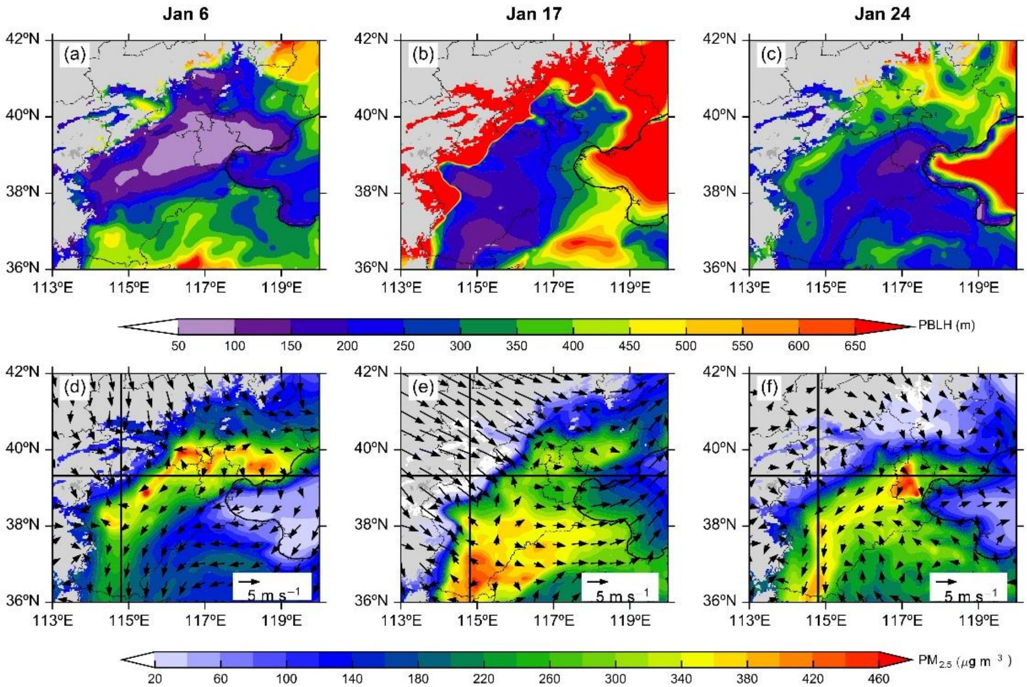
Jan 6
Jan 17
Jan 24
(a)
(b)
(c)
(d)
(e)
(f)
42ºN
40ºN
38ºN
36ºN
113ºE
115ºE
117ºE
119ºE
5 m s⁻¹
PBLH (m)
50 100 150 200 250 300 350 400 450 500 550 600 650
PM2.5 (μg m⁻³)
20 60 100 140 180 220 260 300 340 380 420 460

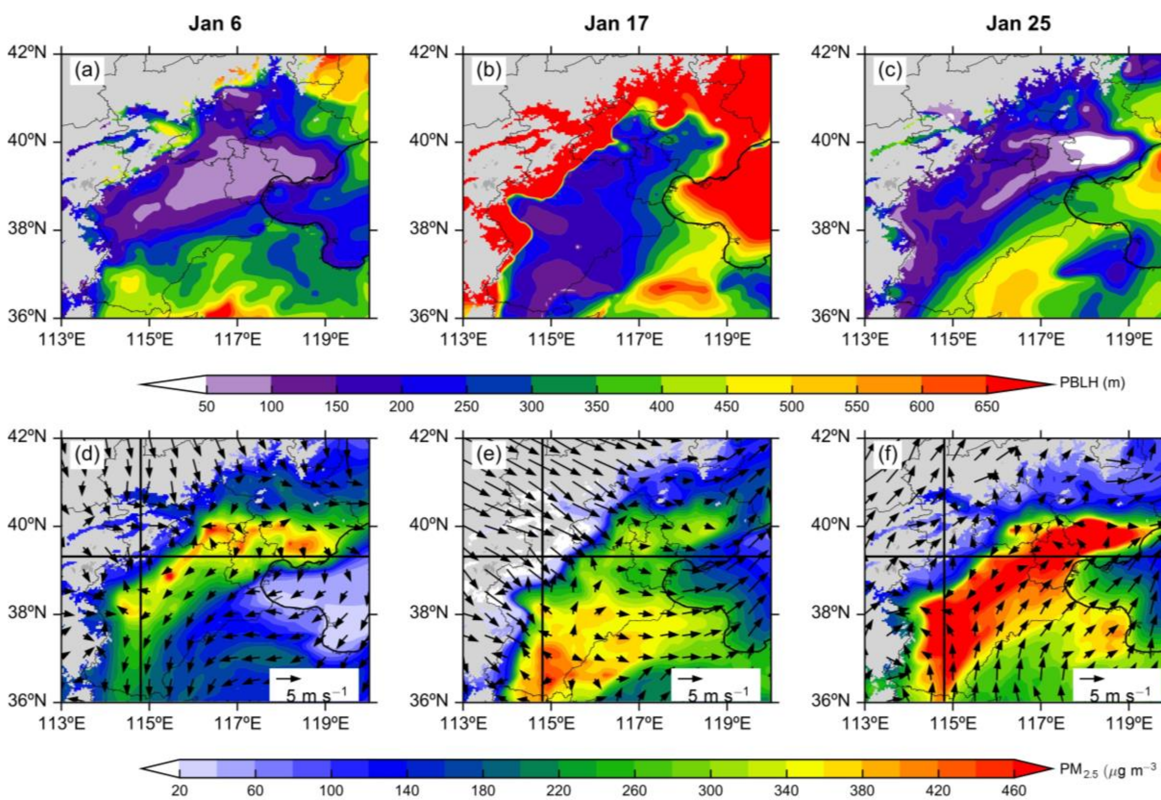
Jan 6
Jan 17
Jan 25
(a)
(b)
(c)
(d)
(e)
(f)
42ºN
40ºN
38ºN
36ºN
113ºE
115ºE
117ºE
119ºE
5 m s⁻¹
PBLH (m)
50 100 150 200 250 300 350 400 450 500 550 600 650
PM2.5 (μg m⁻³)
20 60 100 140 180 220 260 300 340 380 420 460

Figure 6. Distribution of simulated (CTL) daytime (09:00–16:00 BJT) PBLH (a–c), near-surface $PM_{2.5}$ concentrations (d–f: shading), and wind vectors at 10 m (d–f: black arrow) on January 6, 17, and 25~~4~~. The grey shading denotes the terrain height over 1000 m. The black lines indicate the location of the vertical cross-sections shown in Figures 7, 9–12~~0~~.

3.3 Influence of local circulations on pollutant distribution

Under these~~ similar~~ weak weather-scale systems, local circulation may dominate the distribution of pollutants and the development of haze. Figure 7 displays the daytime vertical circulation vectors and $PM_{2.5}$ concentrations along the west-east (to the east of the Taihang Mountains) cross-~~–~~section and along the south-north (to the south of the border between the Taihang and Yanshan Mountains) cross-~~–~~section respectively on the three days. For the cross-section along west-east, ~~the~~a clockwise vertical circulation was formed in the lower level on January 6.~~ vertical circulation was similar on January 6 and 24:~~ T~~t~~he westerly airflow sharply weakened after crossing the mountains, and the zonal wind speeds at lower levels (< 500 m, where the pollution was most severe) were mostly below 2 m s^{-1}; the differential heating between the mountain slopes and the plains caused the atmosphere on the slopes to rise with relative heating and the atmosphere on the plains to sink with relative cooling, resulting in a weak clockwise local circulation between the eastern Taihang Mountains and the BTH plain (119 ° E) (Fig. 7a~~, c~~);~~.~~ ~~P~~pollutants then accumulated in the PBL through this recirculation.~~, and their concentration distribution was closely related to the scale and location of the circulation~~. ~~Compared to January 24, the circulation was lower (< 300 m) but more eastward (about 119 ° E) on January 6, so the high $PM_{2.5}$ concentrations were concentrated at lower altitudes but more widely west-east.~~ There was a similar vertical circulation on January 25 (Fig. 7c). However, this circulation was limited (between the eastern Taihang Mountains and 118 ° E) due to the control of lower and near-surface southwesterly winds. On January 17, although a sinking motion occurred within the PBL, the zonal wind speeds were larger throughout the layer compared to the other two days, mostly ranging between 2 to 5 m s^{-1} (Fig. 7b). The stronger westerly winds made it relatively easy for pollutants to disperse eastward, thus the $PM_{2.5}$ concentrations were lower than those on the other two days. For the cross-section along south-north, the $PM_{2.5}$ concentrations on January 6 were significantly lower than those on January 17 and 25~~4~~. On January 6, northeasterly winds prevailed near the surface of the center and southern BTH, and the pollutants were transported from northeast to southwest via this channel (Fig. 6d); the airflow over the mountains formed a whole layer of subsidence near 38 ° N (Fig. 7d), which inhibited the upward transport of pollutants; at the same time, there was a vertical local circulation at 33–37 °N, between 700 and 1500 m (Fig. 7d), which made pollutants recirculate in this region and not easily disperse to the outside. However, due to the high altitude of this circulation, its restrictions on pollutants were not as strong as the zonal circulations on January 6 (Fig. 7a) and 25~~4~~ (Fig. 7c). On January 17, a wind convergence zone accompanied by sinking motion existed in the lower levels (< 1000 m) near 37 ° N (Fig. 7e). The combined effect of southerly and northerly winds made the pollutants difficult to disperse outward, thus accumulating locally. On January 25~~4~~, southerly winds prevailed throughout the layer below 1500 m~~a clockwise circulation was located between the southern slopes of the mountains and the plains north of 35 ° N~~ (Fig. 7f), which is a typical meteorological condition leading severe air pollution in this region (Huang et al., 2020; Zhang et al., 2019; Zhong et al., 2018b).~~,~~ ~~with its~~

center at about 700 m; Southerly winds prevailed throughout the layer south of 35°N. Thus, airThis southerly winds facilitated local pollutants accumulation by weaken their horizontal diffusion and bring in warm and humid air mass. recirculated and accumulated by the superposition of the lower circulation and southerly winds.

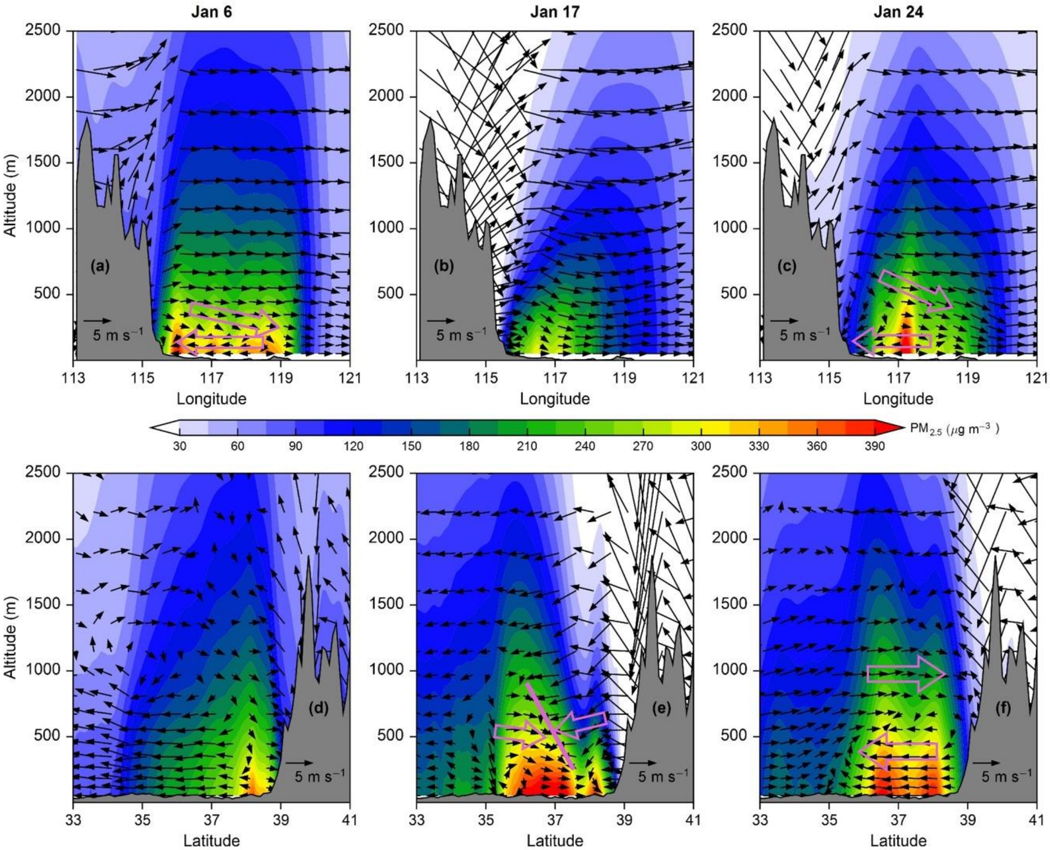
Jan 6
Jan 17
Jan 24
Altitude (m)
2500
2000
1500
1000
500
(a)
(b)
(c)
(d)
(e)
(f)
5 m s^{-1}
113
115
117
119
121
Longitude
PM$_{2.5}$ (μg m^{-3})
30
60
90
120
150
180
210
240
270
300
330
360
390
33
35
37
39
41
Latitude

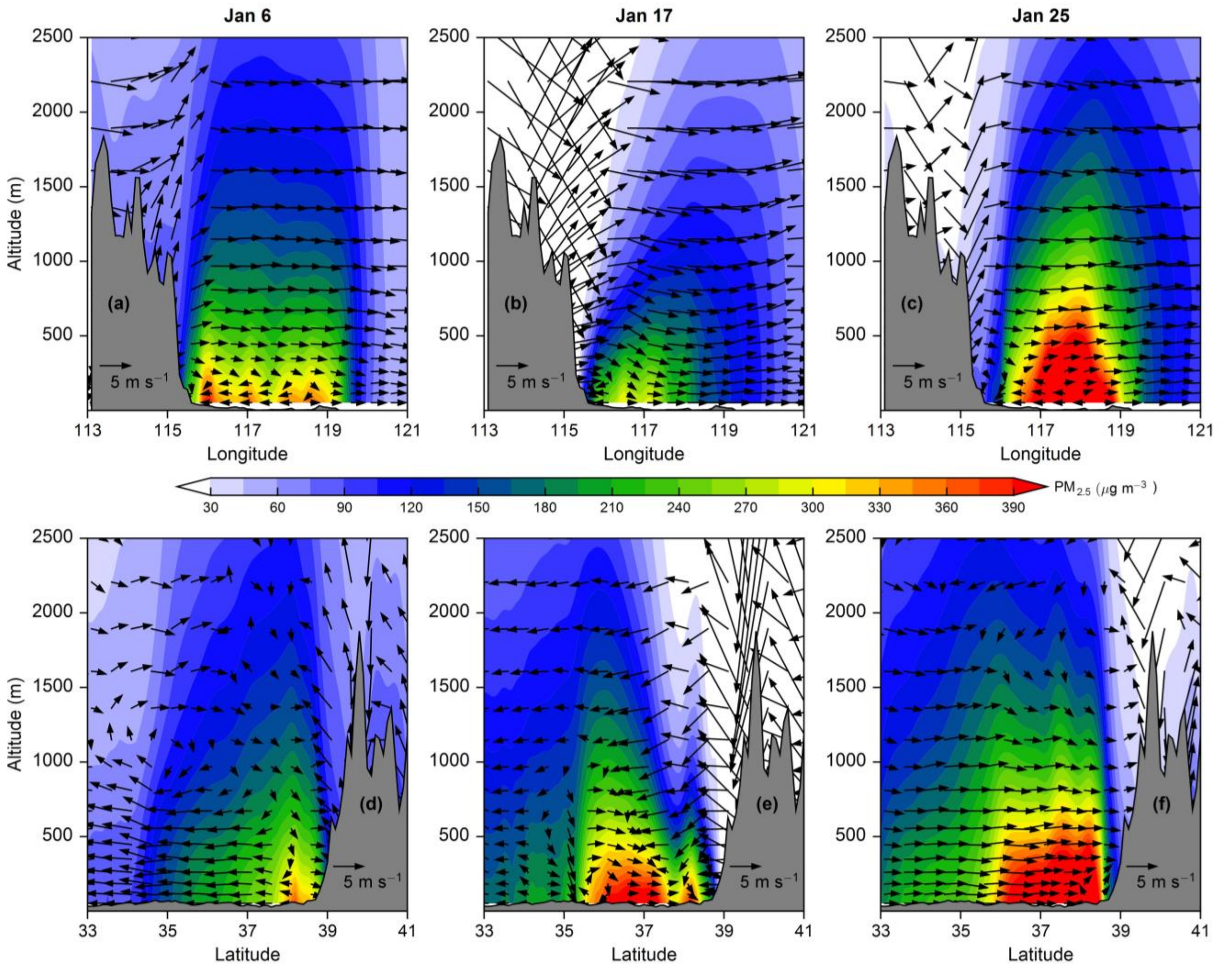

Figure 7. Vertical cross-section of simulated (CTL) wind field (a–c: zonal wind and 100 times of vertical velocity; d–f: meridional wind and 100 times of vertical velocity) and $PM_{2.5}$ concentrations during daytime (09:00–16:00 BJT) on January 6, 17, and 25~~4~~. ~~Rose arrow indicates the direction of airflow, and rose line indicates the wind convergence line.~~

3.4 Amplification of local circulations on heavy haze by ARI

Given the considerable impacts of local circulation and ARI on the distribution of $PM_{2.5}$ extremes, we further analysed the potential link between them~~air pollutants and the influence of ARI on the vertical structure of the PBL, it is necessary to further analyze the possible impacts of ARI on local~~. According to the location of the cross-sections in Fig. S3, Fig. 8 shows the vertical distribution of wind field and $PM_{2.5}$ with and without the ARI mechanism and the difference of horizontal wind speeds induced by ARI. For the cross-section along west-east, ARI strengthened the clockwise vertical circulation near 500 m by simultaneously enhancing the westerly winds in the upper level (500~1000 m) and the easterly winds in the lower level (< 500 m) (Fig. 8a–c). For the cross-section along south-north, ARI strengthened the circulation at high altitude between 33 and 35 ° N by enhancing the upper (900~1500 m) southerly winds and the lower (< 500 m) northerly winds (Fig. 8d–f). Moreover, the southerly winds in the circulation formed a wind convergence zone with the northerly winds on its north side (Fig. 8d–e), and ARI strengthened this zone by increasing the wind on both sides (Fig. 8f).

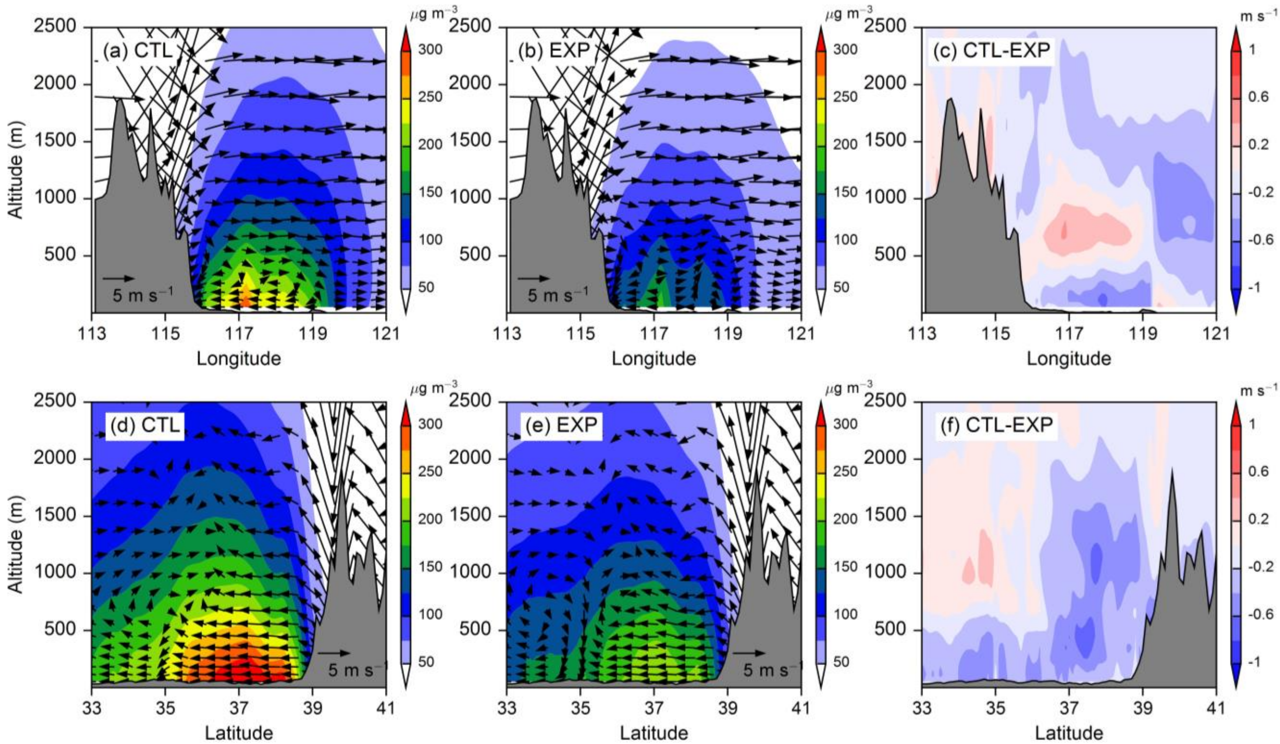

Figure 8. Vertical cross-section of simulated (CTL and EXP) daytime (09:00–16:00 BJT) wind field (a–b: zonal wind and 100 times of vertical velocity; d–e: meridional wind and 100 times of vertical velocity) and $PM_{2.5}$ concentrations, and the differences (CTL-EXP) of horizontal wind (c: zonal wind; f: meridional wind) induced by ARI during the three pollution periods.

As the local circulation characteristics were different on the three heavy haze days (Fig. 7), it was necessary to investigate the impact of ARI on each day. As shown in Figs. ~~8~~9–1~~1~~2, the impacts~~effects~~ of ARI on circulations could be broadly classified into two types: strengthened local circulation and weakened horizontal diffusion~~transport~~. First, ARI significantly strengthened the vertical zonal circulations on January 6 and 25~~4, particularly for the zonal circulations~~: the high aerosol concentrations concentrated on the BTH plain during the daytime substantially cooled the lower atmosphere by absorbing and scattering solar radiation, and the widening difference in atmospheric heating between the mountain slopes and the BTH plain led to a simultaneous strengthening of westerly winds in the upper level and easterly winds in the lower level (Fig. 8a, c). On January 6, between the eastern Taihang Mountains and 119 °E, ARI increased the westerly winds (300–~800 m) and the easterly winds (< 300 m) by 0.8 and 0.3 m s^{-1}, respectively, on average (Figs. 9a, 11a, 11d). On January 254, ARI increased the westerly winds by 0.6 m s^{-1} at the same location as on January 6; meanwhile, the airflow below 300 m changed from weak westerly to easterly under the ARI effect, forming a closed circulation with the upper westerly winds (Figs. 9c, 11c, 11f).(400–900 m) between the eastern Taihang Mountains and 119 °E by 0.7 m s^{-1}, and easterly winds (< 300 m) west of 117 °E by 0.2 m s^{-1}; at the same time, ARI decreased the westerly winds (< 300 m) between 117 and 119 °E by 0.3 m s^{-1}, which hindered the eastward transport of aerosols. Moreover, ARI could change the altitude of circulation. On January 6, ARI shifted the vertical circulation downward by about 100 m according to the wind speed minimum and the height of the wind shear (Fig. 110a, d). The stronger and lower vertical circulation caused further accumulation of pollutants in the lower level, which then led to substantial cooling of the lower atmosphere (Fig. 98d, f) and weak vertical turbulent diffusion (Fig. 98g, i). ARI also strengthened the meridional circulations on January 6 and 24, although it did not cause the same downshift as the zonal circulations.: Due to the ARI effect, the southerly winds in the upper level and the northerly winds in the lower level were strengthened simultaneously (Figs. 109a, 12a, 12de); the strengthened vertical circulation in this local area likewise traps the pollutants in the limited space, which further cooled atmosphere (Fig. 109d, f) and weakened turbulent diffusion (Fig. 109g, i) in lower atmosphere.

Second, ARI weakened the horizontal diffusion of pollutantstransport. on January 17. For the relatively lightly polluted northern BTH on January 17, ARI weakened the westerly winds below 300 m and east of 117 °E (Figs. 98b, 11b, 11e), with a maximum wind speed reduction of 1 m s^{-1}. In addition, ARI enhanced the sinking of airflow near 116 °E (Fig. 11b, e), promoting the accumulation of aerosols in the lower layer. For the heavily severe polluted southern BTH on January 17, ARI enhanced the wind convergence zone near 37 °N (Fig. 11b) by simultaneously strengthening the southerly winds south of the convergence line and the northerly winds north of the convergence line (Figs. 10b, 12b, 12e)(Fig. 9b). At the same time, ARI pushed this convergence line northward, causing southerly winds to prevail below 200 m over the plain. In addition, ARI enhanced the southerly winds below 600 m along south-north on January 25 (Figs. 10c, 12c, 12f), with an average increase of 0.6 m s^{-1}. Pollutants accumulated locallycould not be transported northward due to the blockage of the Yanshan Mountains,. Both of these weakened the horizontal transport of pollutants, which thenand thus the highly concentrated pollutants led to cooling of the lower atmosphere (Figs. 8e10 and 9e–f) and weakening of the vertical turbulent motion (Figs. 8h10 and 9h–i)., just like January 6 and 24.

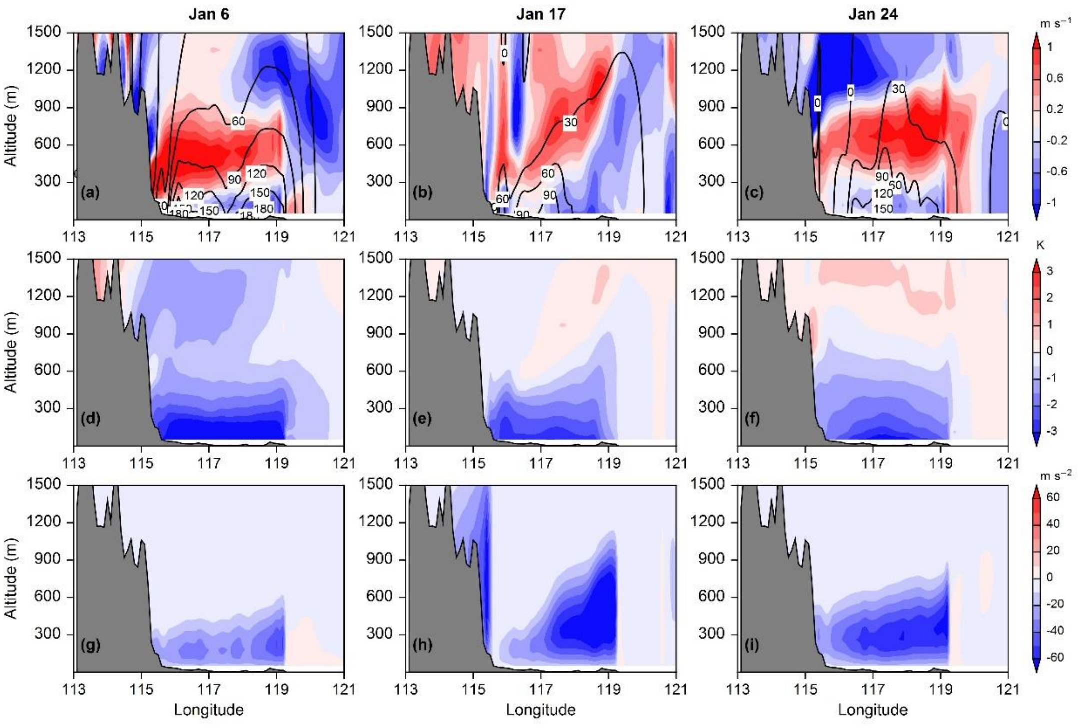

Jan 6
Jan 17
Jan 24
Altitude (m)
Longitude
(a)
(b)
(c)
(d)
(e)
(f)
(g)
(h)
(i)
m s⁻¹
K
m s⁻²

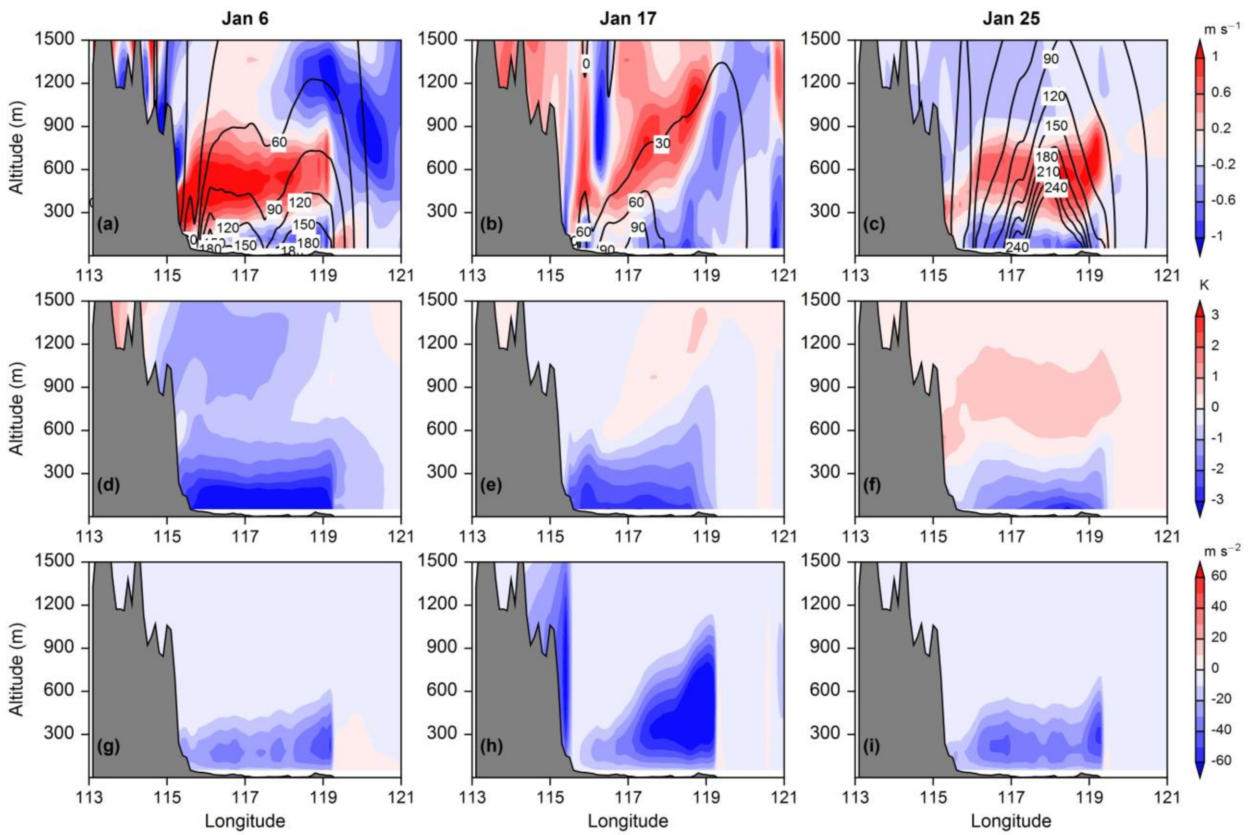

Figure 9~~8~~. Vertical cross-section of simulated (a–c) zonal wind (shading) and $PM_{2.5}$ concentration (contour: μg m^{-3}), (d–f) PT, and (g–i) vertical turbulent diffusion coefficient differences (CTL–EXP) induced by ARI~~aerosol-radiation feedbacks~~ during daytime (09:00–16:00 BJT) on January 6, 17, and 25~~4~~.

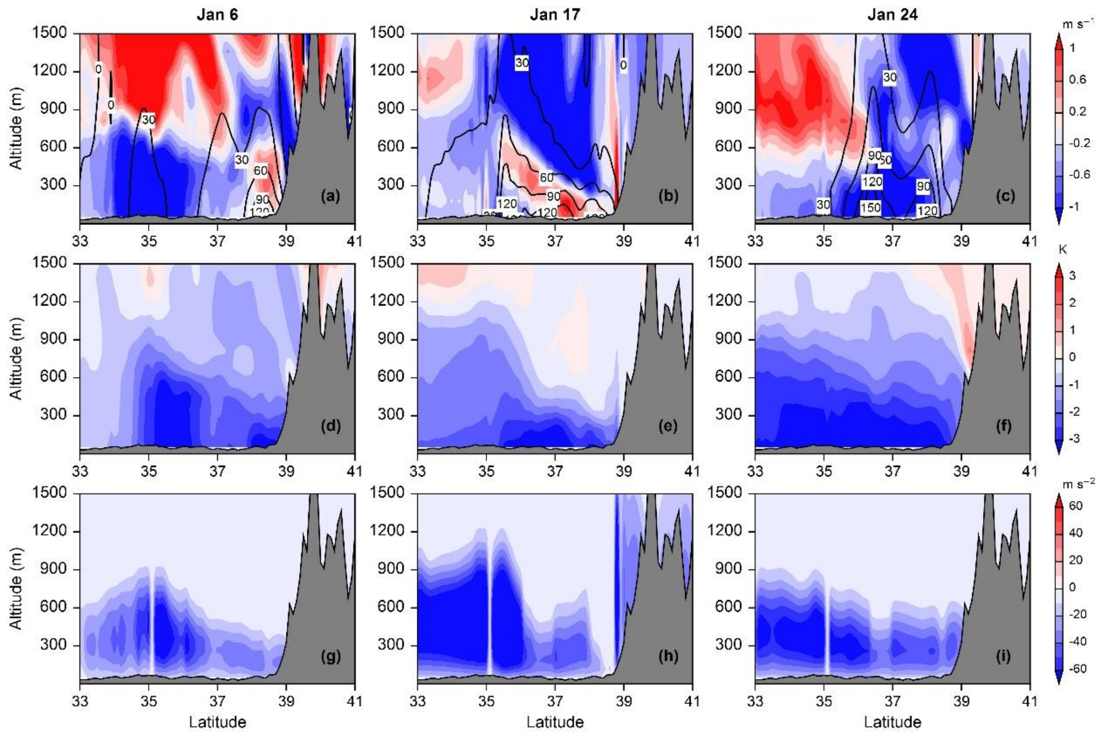
Jan 6
Jan 17
Jan 24
Altitude (m)
Latitude
(a)
(b)
(c)
(d)
(e)
(f)
(g)
(h)
(i)
m s⁻¹
1
0.6
0.2
-0.2
-0.6
-1
K
3
2
1
0
-1
-2
-3
m s⁻²
60
40
20
0
-20
-40
-60

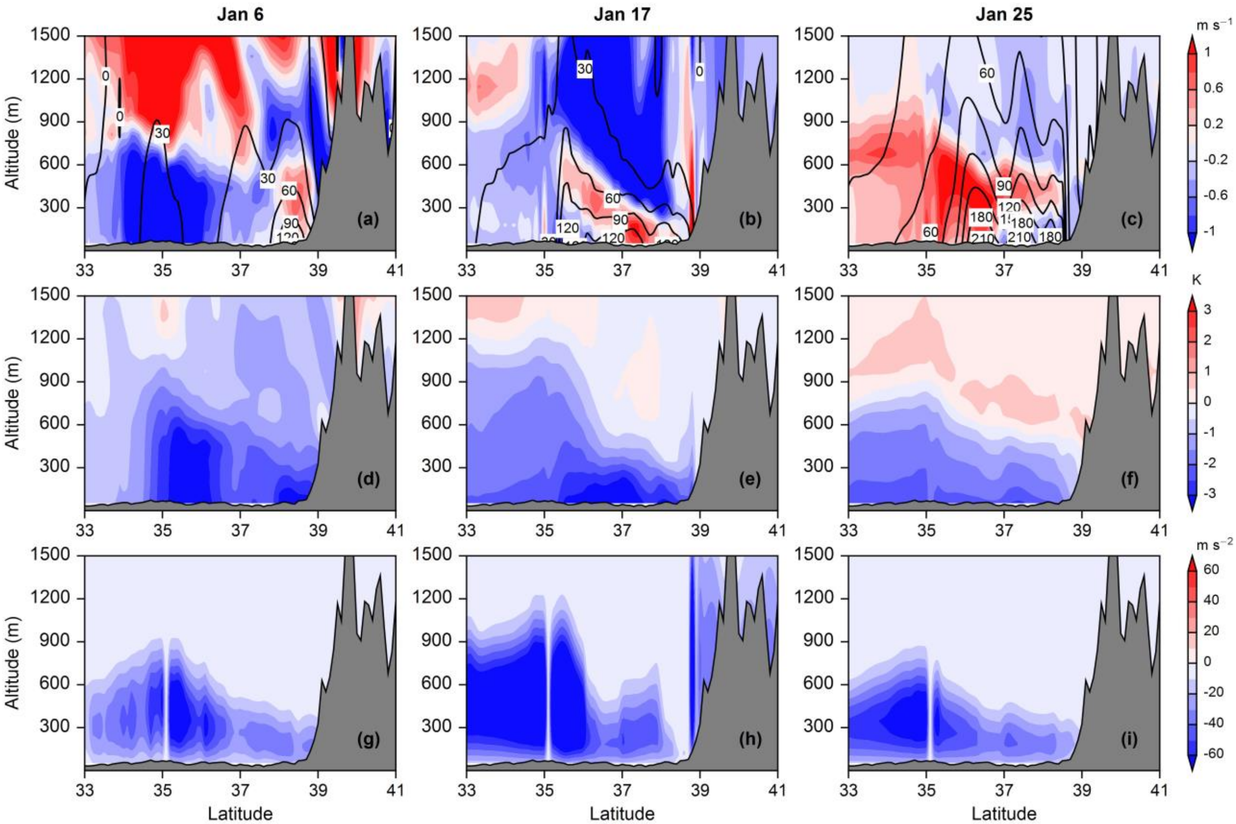

Figure 109. Vertical cross-section of simulated (a–c) meridional wind (a–c: shading), $PM_{2.5}$ concentration (a–c: contours,: μg m^{-3}), (d–f) PT (d–f), and (g–i) vertical turbulent diffusion coefficient differences (CTL–EXP) induced by aerosol-radiation feedbacksARI during daytime (09:00–16:00 BJT) on January 6, 17, and 254.

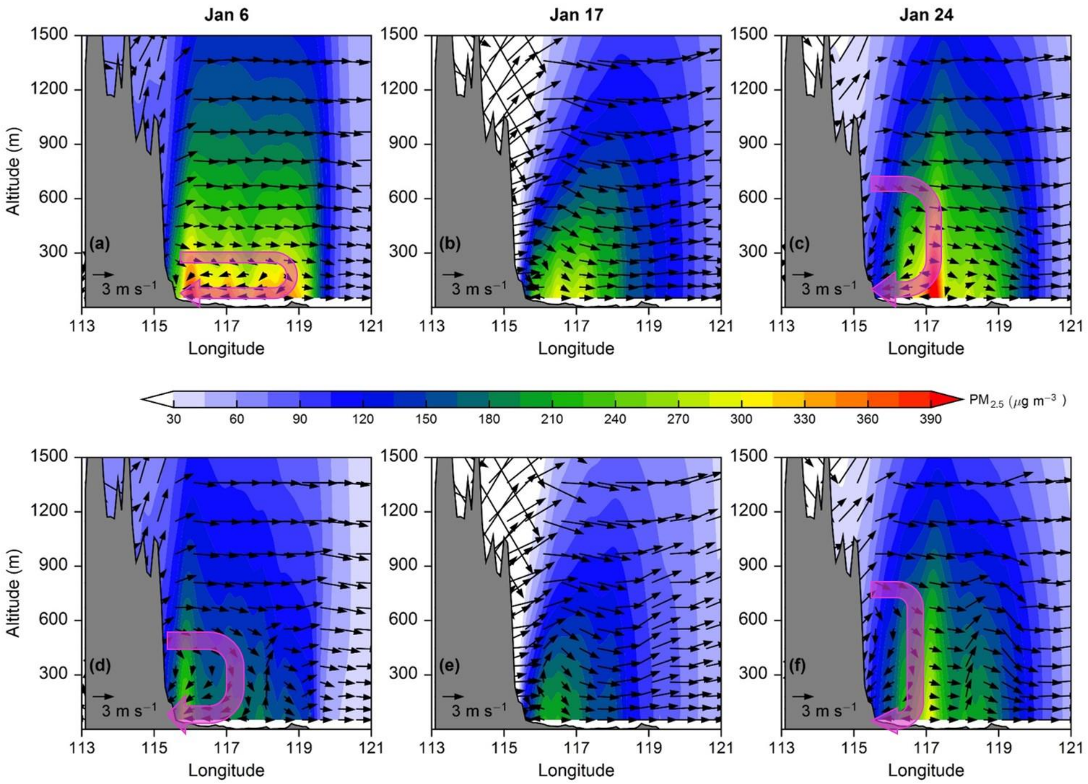

Jan 6
Jan 17
Jan 24
Altitude (m)
Longitude
(a)
(b)
(c)
(d)
(e)
(f)
3 m s^{-1}
PM$_{2.5}$ (μg m^{-3})

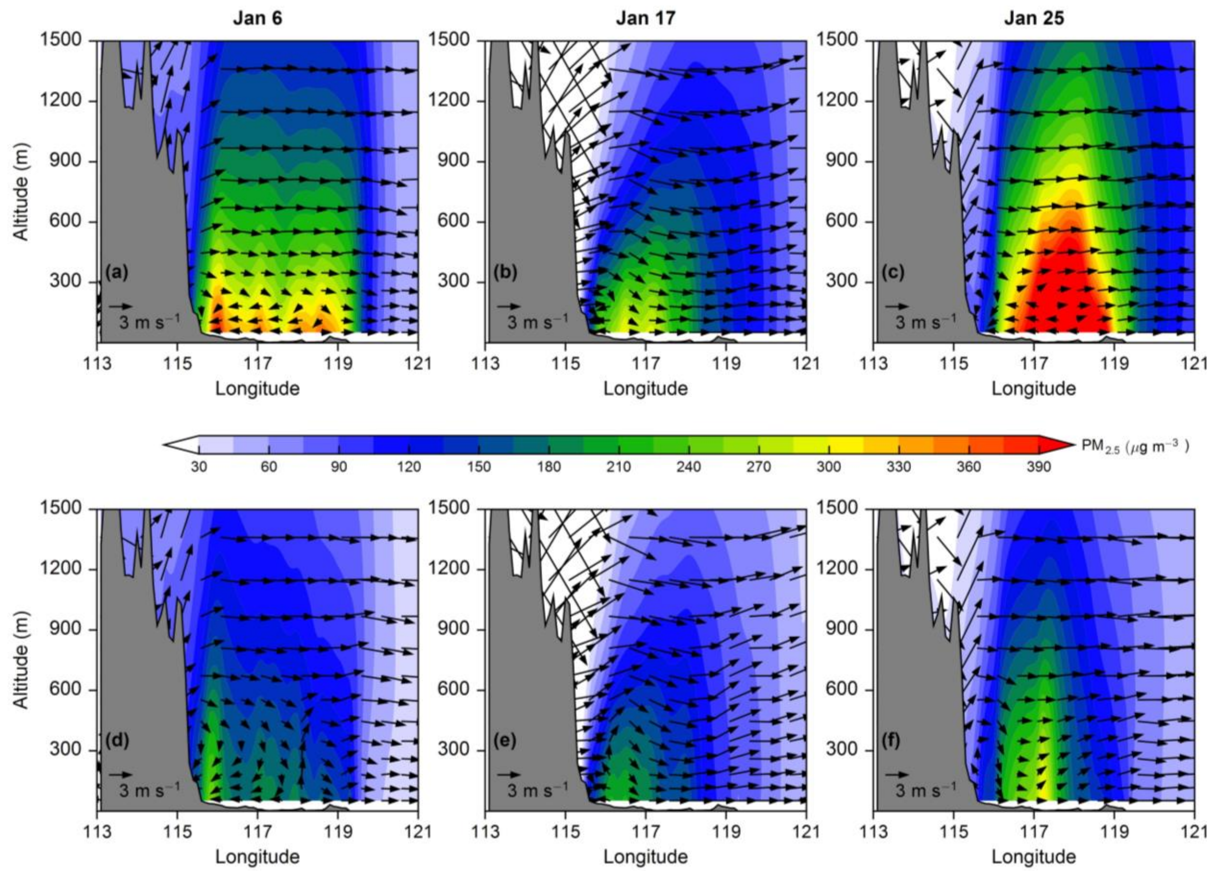

Figure 1<u>1</u>~~0~~. Vertical cross-section of simulated wind field (zonal wind and 100 times of vertical velocity) and $PM_{2.5}$ concentrations from (a–c) CTL and (d–f) EXP during daytime (09:00–16:00 BJT) on January 6, 17, and 2<u>5</u>~~4~~. ~~Rose arrow indicates the general location of the vertical circulation.~~

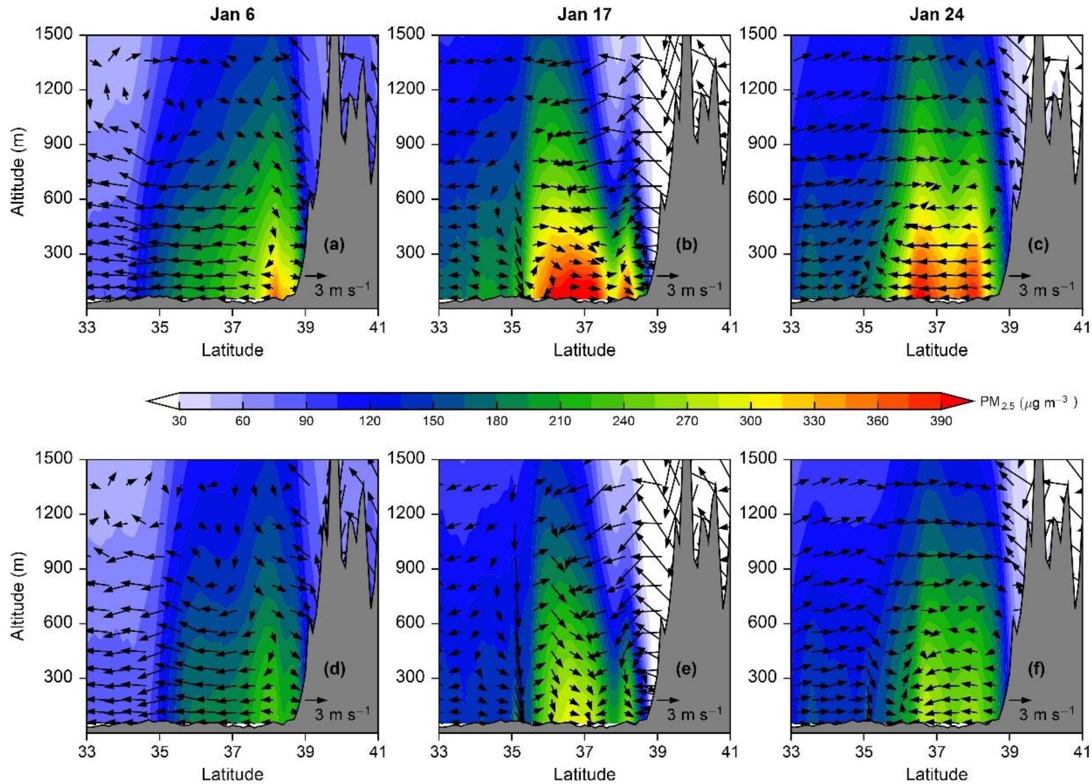
Jan 6
Jan 17
Jan 24
Altitude (m)
Latitude
(a)
(b)
(c)
(d)
(e)
(f)
3 m s⁻¹
PM 2.5 (μg m⁻³)

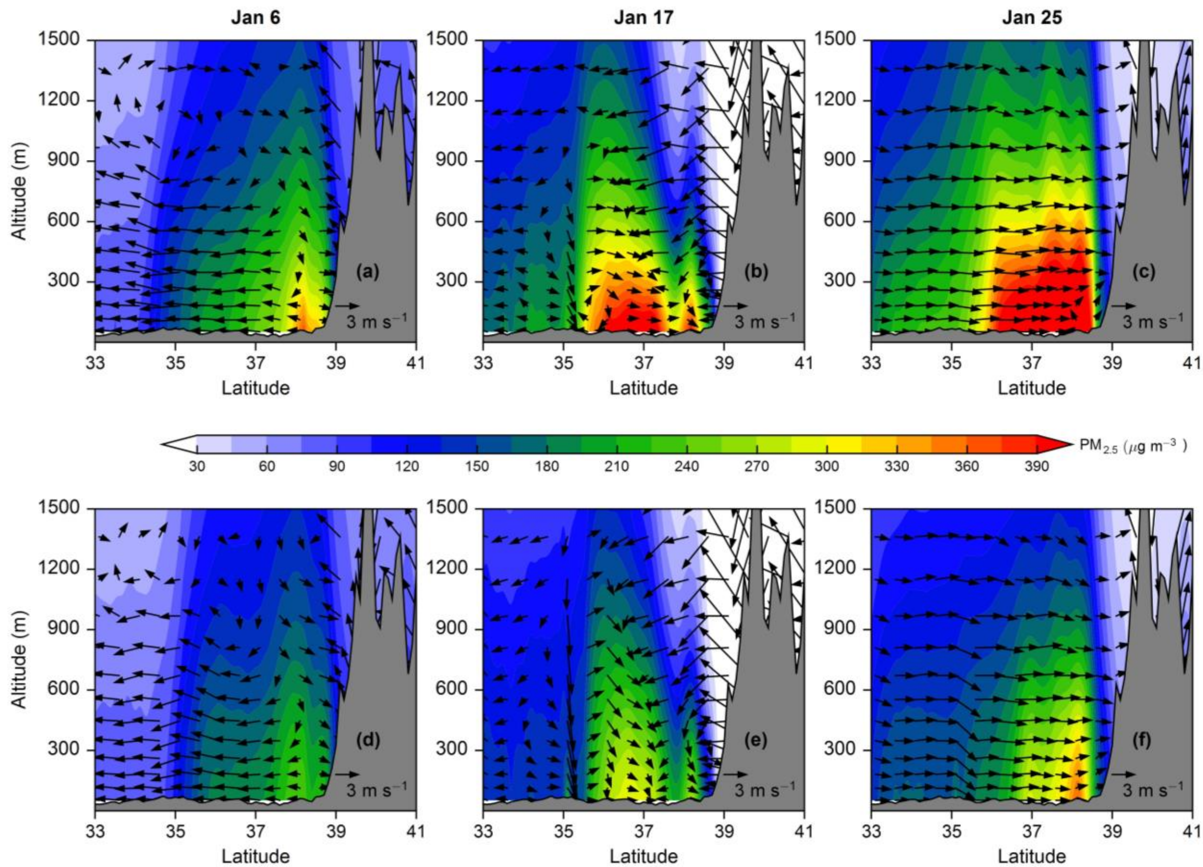

Figure 12~~1~~. Vertical cross-section of simulated wind field (meridional wind and 100 times of vertical velocity) and $PM_{2.5}$ concentrations from (a–c) CTL and (d–f) EXP during daytime (09:00–16:00 BJT) on January 6, 17, and 2~~4~~5.

4 Conclusions

In this study, the link between aerosol, local vertical circulation, and heavy haze pollution in the BTH plain in winter was investigated, based on surface and sounding observations and simulation experiments by the atmospheric chemistry model GRAPES_Meso5.1/CUACE in January 2017.

From synoptic perspective, the appropriate configurations of the upper, middle, and lower levels provided favorable conditions for the accumulation of pollutants. During the haze pollution, the BTH region was mainly controlled by the zonal westerly airflow or northwesterly airflow ~~in front of the high pressure ridge~~ in~~at~~ the upper and middle troposphere~~levels~~, and the most polluted central and southern BTH was often dominated by the southwesterly winds in~~at~~ the lower troposphere~~levels~~; at the same time, the blockage of the Taihang and Yanshan Mountains significantly weakened airflow from the west and north, while hindering the northward and westward transport of pollutants.

Under these unfavorable synoptic conditions, the typical local circulation induced by the mountainous topography played a key role in the heavy haze pollution. During the daytime on ~~the selected~~ haze~~pollution~~ days, ~~the differential heating induced by mountainous topography led to the formation of~~a local closed vertical circulation ~~and~~or wind convergence zone was formed in the lower atmosphere between the mountain slopes and the BTH plain under the influence of the mountainous topography, which was not conducive to the pollutant vertical and horizontal diffusion.~~ and horizontal transport of the pollutants and led to their recirculation and accumulation in local areas.~~ Both the intensity~~size~~ and location of the vertical circulation played an important role in the pollutant distribution. The~~A smaller-scale, lower-altitude~~ circulation with high intensity and low altitude could constrain near-surface pollutants to a more limited area. More importantly, the superposition of the ARI mechanism and local circulation could significantly aggravate haze pollution. According to the simulation results of this study, ARI mainly amplified the impacts of local vertical circulation on haze in ~~the~~ two ways: strengthening local circulation and weakening horizontal diffusion~~transport~~. For the clockwise vertical circulation~~ along west-east~~, ARI not only strengthened both the upper westerly winds and the lower easterly winds, but also pressed the circulation toward~~down~~ to the lower atmosphere; for the wind convergence~~ formed along south-north~~ zone, ARI strengthened the southerly and northerly winds on both sides of the convergence line~~,~~ and simultaneously pushed~~made~~ the convergence line move northward. ~~Through the above two pathways,~~ ARI amplified the inhibitory of local circulation on vertical and horizontal diffusion of pollutants through these two pathways~~ and horizontal transport~~, leading to pollutants recirculating~~trapping pollutants~~ in a more limited space. With the superposition of ARI and local circulation, aerosols accumulated rapidly in the lower atmosphere, which led to more stable atmospheric stratification and subsequent deterioration of haze pollution.

Data availability

All raw data can be provided by the corresponding authors upon request.

Author contribution

HW and XZ conceived the idea; YP and HW designed the experiment; YP ran the model and wrote the manuscript draft; ZL and WZ provided the observation data and helped perform the analysis with constructive discussions; YP, SL, and CH analysed the data; YP, HW, and HC reviewed and edited the manuscript.

Competing interests

The authors declare that they have no conflict of interest.

Financial support

This work was supported by the NSFC Major Project (42090030), the National Key Research and Development Program of China (2019YFC0214601), and the NSFC for Distinguished Young Scholars (41825011).

References

Boylan, J. W., Russell, A. G.: PM and light extinction model performance metrics, goals, and criteria for three-dimensional air quality models, Atmos. Environ., 40, 4946–4959, https://doi.org/10.1016/j.atmosenv.2005.09.087, 2006.

Chen, D. H., Xue, J. S., Yang, X. S., Zhang, H. L., Shen, X. S., Hu, J. L., Wang, Y., Ji, L. R., and Chen, J. B.: New generation of multi-scale NWP system (GRAPES): general scientific design, Chin. Sci. Bull., 53, 3433–3445, https://doi.org/10.1007/s11434-008-0494-z, 2008.

Chen, Y., Zhao, C., Zhang, Q., Deng, Z., Huang, M., and Ma, X.: Aircraft study of mountain chimney effect of Beijing, China, J. Geophys. Res., 114, D08306, https://doi.org/10.1029/2008JD010610, 2009.

Chou, M. D., Suarez, M. J., Ho, C. H., Yan, M. M. H., and Lee, K. T.: Parameterizations for cloud overlapping and shortwave single-scattering properties for use in general circulation and cloud ensemble models, J. Clim., 11, 202–214, 1998.

Ding, A. J., Huang, X., Nie, W., Sun, J. N., Kerminen, V. M., Petäjä, T., Su, H., Cheng, Y. F., Yang, X.-Q., Wang, M. H., Chi, X. G., Wang, J. P., Virkkula, A., Guo, W. D., Yuan, J., Wang, S. Y., Zhang, R. J., Wu, Y. F., Song, Y., Zhu, T., Zilitinkevich, S., Kulmala, M., and Fu, C. B.: Enhanced haze pollution by black carbon in megacities in China, Geophys. Res. Lett., 43(6), 2873–2879, https://doi.org/10.1002/2016GL067745, 2016.

Ek, M. B., Mitchell, K. E., Lin, Y., Rogers, E., Grunmann, P., Koren, V., Gayno, G., and Tarpley, J. D.: Implementation of Noah land surface model advances in the National Centres for Environmental Prediction operational mesoscale Eta model, J. Geophys. Res., 108 (D22), 8851, https://doi.org/10.1029/2002JD003296, 2003.

Fu, G. Q., Xu, W. Y., Yang, R. F., Li, J. B., and Zhao, C. S.: The distribution and trends of fog and haze in the North China Plain over the past 30 years, Atmos. Chem. Phys., 14, 11949–11958, https://doi.org/10.5194/acp-14-11949-2014, 2014.

Gao, M., Liu, Z., Wang, Y., Lu, X., Ji, D., and Wang, L.: Distinguishing the roles of meteorology, emission control measures, regional transport, and co-benefits of reduced aerosol feedback in “APEC” Blue, Atmos. Environ., 167, 476–486, https://doi.org/10.1016/j.atmosenv.2017.08.054, 2017.

Gong, S. L., and Zhang, X. Y.: CUACE/Dust – an integrated system of observation and modeling systems for operational dust forecasting in Asia, Atmos. Chem. Phys., 8, 2333–2340, 2008.

Hong, S. Y., and Pan, H. L.: Nonlocal boundary layer vertical diffusion in a medium-range forecast model, Mon. Weather Rev., 124, 2322, 1996.

Huang, X., Ding, A., Wang, Z. Ding, K., Gao, J., Chai, F., and Fu, C.: Amplified transboundary transport of haze by aerosol–boundary layer interaction in China, Nat. Geosci., 13, 428–434, https://doi.org/10.1038/s41561-020-0583-4, 2020.

Huang, X., Wang, Z., and Ding, A.: Impact of aerosol-PBL interaction on haze pollution: Multiyear observational evidences in North China, Geophys. Res. Lett., 45(16), 8596–8603, https://doi.org/10.1029/2018GL079239, 2018.

Kain, J. S.: The Kain-Fritsch convective parameterization: An update, J. Appl. Meteor., 43, 170–181, 2004.

Mlawer, E. J., Taubman, S. J., Brown, P. D., Iacono, M. J., and Clough, S. A.: Radiative transfer for inhomogeneous atmosphere: RRTM, a validated correlated-k model for the longwave, J. Geophys. Res., 102, 16663-16682, https://doi.org/10.1029/97JD00237, 1997.

Li, Z., Guo, J., Ding, A., Liao, H., Liu, J., Sun, Y., Wang, T., Xue, H., Zhang, H., and Zhu, B.: Aerosol and boundary-layer interactions and impact on air quality, Natl. Sci. Rev., 4, 810–833, https://doi.org/10.1093/nsr/nwx117, 2017.

Liu, Q., Jia, X., Quan, J., Li, J.,Li, X., Wu, Y., Chen, D., Wang, Z., and Liu, Y.: New positive feedback mechanism between boundary layer meteorology and secondary aerosol formation during severe haze events, Sci. Rep., 8, 6095, https://doi.org/10.1038/s41598-018-24366-3, 2018.

Liu, S., Liu, Z., Li, J., Wang, Y., Ma, Y., Sheng, L., Liu, H., Liang, F., Xin, G., and Wang, J.: Numerical simulation for the coupling effect of local atmospheric circulations over the area of Beijing, Tianjin and Hebei Province, Sci. China Ser. D-Earth Sci, 52, 382–392, https://doi.org/10.1007/s11430-009-0030-2, 2009.

Lo, J. C. F., Lau, A. K. H., Fung, J. C. H. and Chen, F.: Investigation of enhanced cross−city transport and trapping of air pollutants by coastal and urban land−sea breeze circulations, J. Geophys. Res., 111, D14104, https://doi.org/10.1029/2005JD006837, 2006.

Mlawer, E. J., Taubman, S. J., Brown, P. D., Iacono, M. J., and Clough, S. A.: Radiative transfer for inhomogeneous atmosphere: RRTM, a validated correlated-k model for the longwave, J. Geophys. Res., 102, 16663–16682, https://doi.org/10.1029/97JD00237, 1997.

Miao, Y., Che, H., Zhang, X., and Liu, S.: Integrated impacts of synoptic forcing and aerosol radiative effect on boundary layer and pollution in the Beijing–Tianjin–Hebei region, China, Atmos. Chem. Phys., 20, 5899–5909, https://doi.org/10.5194/acp-20-5899-2020, 2020.

Miao, Y., Li, J., Miao, S., Che, H., Wang, Y., Zhang, X., Zhu, R., and Liu, S.: Interaction between planetary boundary layer and $PM_{2.5}$ pollution in megacities in China: a Review, Curr. Pollut. Rep., 5(4), 261–271, https://doi.org/10.1007/s40726-019-00124-5, 2019.

Miao, Y., Liu, S., Zheng, Y., Wang, S., Chen, B., Zheng, H., and Zhao, J.: Numerical study of the effects of local atmospheric circulations on a pollution event over Beijing–Tianjin–Hebei, China, J. Environ. Sci, 30, 9–20, http://dx.doi.org/10.1016/j.jes.2014.08.025, 2015.

Morris, R. E., McNally, D. E., Tesche, T. W., Tonnesen, G., Boylan, J. W., and Brewer, P.: Preliminary Evaluation of the Community Multiscale Air Quality Model for 2002 over the Southeastern United States, J. Air Waste Manage. Assoc., 55(11), 1694–1708, https://doi.org/10.1080/10473289.2005.10464765, 2005.

Peng, Y., Wang, H., Hou, M., Jiang, T., Zhang, M., Zhao, T., and Che, H.: Improved method of visibility parameterization focusing on high humidity and aerosol concentrations during fog–haze events: Application in the GRAPES_CAUCE model in Jing-Jin-Ji, China, Atmos. Environ., 222, 117139, https://doi.org/10.1016/j.atmosenv.2019.117139, 2020.

Peng, Y., Wang, H., Zhang, X., Zhao, T., Jiang, T., Che, H., Zhang, X., Zhang, W., and Liu, Z.: Impacts of PBL schemes on $PM_{2.5}$ simulation and their responses to aerosol-radiation feedback in GRAPES_CUACE model during severe haze episodes in Jing-Jin-Ji, China, Atmos. Res., 248, 105268, https://doi.org/10.1016/j.atmosres.2020.105268, 2021.

Peng, Y., Wang, H., Zhang, X., Zheng, Y., Zhang, X., Zhang, W., Liu, Z., Gui, K., Liu, H., Wang, Y., and Che, H.: Aerosol-radiation interaction in the operational atmospheric chemistry model GRAPES_Meso5.1/CUACE and its impacts on mesoscale NWP in Beijing-Tianjin-Hebei, China, Atmos. Res., 280, 106402, https://doi.org/10.1016/j.atmosres.2022.106402, 2022~~under review~~.

Quan, J., Dou, Y., Zhao, X., Liu, Q., Sun, Z., Pan, Y., Jia, X., Cheng, Z., Ma, P., Su, J., Xin, J., and Liu, Y.: Regional atmospheric pollutant transport mechanisms over the North China Plain driven by topography and planetary boundary layer processes, Atmos. Environ., 221, 117098, https://doi.org/10.1016/j.atmosenv.2019.117098, 2020.

Quan, J., Gao, Y., Zhang, Q., Tie, X., Cao, J., Han, S., Meng, J., Chen, P., and Zhao, D.: Evolution of planetary boundary layer under different weather conditions, and its impact on aerosol concentrations, Particuology, 11(1): 34–40, http://dx.doi.org/10.1016/j.partic.2012.04.005, 2013.

Stockwell, W. R., Middleton, P., Chang, J. S., and Tang, X.: The second generation regional acid deposition model chemical mechanism for regional air quality modeling, J. Geophys. Res., 95, 16343–16367, https://doi.org/10.1029/JD095iD10p16343, 1990.

Sun, Y., Song, T., Tang, G., and Wang, Y.: The vertical distribution of $PM_{2.5}$ and boundary-layer structure during summer haze in Beijing, Atmos. Environ., 74, 413–421, https://doi.org/10.1016/j.atmosenv.2013.03.011, 2013.

Thompson, G., Field, P. R., Rasmussen, R. M., and Hall, W. D.: Explicit Forecasts of Winter Precipitation Using an Improved Bulk Microphysics Scheme. Part II: Implementation of a New Snow Parameterization, Mon. Weather Rev., 136, 5095–5115, https://doi.org/10.1175/2008MWR2387.1, 2008.

Wang, D., Jiang, B., Lin, W., and Gu, F.: Effects of aerosol-radiation feedback and topography during an air pollution event over the North China Plain during December 2017, Atmos. Pollut. Res., https://doi.org/10.1016/j.apr.2018.10.006, 2019.

Wang, H., Gong, S., Zhang, H., Chen, Y., Shen, X., Chen, D., Xue, J., Shen, Y., Wu, X., and Jin, Z.: A new-generation sand and dust storm forecasting system GRAPES_CUACE/Dust: Model development, verification and numerical simulation, Chin. Sci. Bull., 55(7), 635–649, https://doi.org/10.1007/s11434-009-0481-z, 2010.

Wang, H., Peng, Y., Zhang, X., Liu, H., Zhang, M., Che, H., Cheng, Y., and Zheng, Y.: Contributions to the explosive growth of $PM_{2.5}$ mass due to aerosol–radiation feedback and decrease in turbulent diffusion during a red alert heavy haze in Beijing–Tianjin–Hebei, China,. Atmos. Chem. Phys., 18, 17717–17733, https://doi.org/10.5194/acp-18-17717-2018, 2018.

Wang, H., Shi, G. Y., Zhang, X. Y., Gong, S. L., Tan, S. C., Chen, B., Che, H. Z., and Li, T.: Mesoscale modelling study of the interactions between aerosols and PBL meteorology during a haze episode in China Jing–Jin–Ji and its near surrounding region – Part 2: Aerosols' radiative feedback effects, Atmos. Chem. Phys., 15, 3277–3287, https://doi.org/10.5194/acp-15-3277-2015, 2015b.

Wang, H., Xue, M., Zhang, X. Y., Liu, H. L., Zhou, C. H., Tan, S. C., Che, H. Z., Chen, B., and Li, T.: Mesoscale modeling study of the interactions between aerosols and PBL meteorology during a haze episode in Jing–Jin–Ji (China) and its nearby surrounding region – Part 1: Aerosol distributions and meteorological features, Atmos. Chem. Phys., 15, 3257–3275, https://doi.org/10.5194/acp-15-3257-2015, 2015a.

Wang, H., Zhang, X. Y., Wang, P., Peng, Y., Zhang, W., Liu, Z., Han, C., Li, S., Wang, Y., Che, H., Huang, L., Liu, H., Zhang, L., Zhou, C., Ma, Z., Chen, F., Ma, X., Wu, X., Zhang, B., and Shen, X.: Chemistry-Weather Interacted Model System GRAPES_Meso5.1/CUACE CW V1.0: Development, Evaluation and Application in Better Haze-fog Prediction in China, J. Adv. Model. Earth Syst., 14, e2022MS003222, https://doi.org/10.1029/2022MS003222, 2022.under review.

Wu, P., Ding, Y. H., and Liu, Y. J.: Atmospheric circulation and dynamic mechanism for persistent haze events in the Beijing–Tianjin–Hebei region, Adv. Atmos. Sci., 34(4), 429–440, https://doi.org/10.1007/s00376-016-6158-z, 2017.

Zhang, B., Wang, Y., and Hao, J.: Simulating aerosol–radiation–cloud feedbacks on meteorology and air quality over eastern China under severe haze conditions in winter, Atmos. Chem. Phys., 15, 2387–2404, https://doi.org/10.5194/acp-15-2387-2015, 2015.

Zhang, D., and Anthes, R. A.: A high-resolution model of the planetary boundary layer—sensitivity tests and comparisons with SESAME-79 data, J. Appl. Meteorol., 21, 1594–1609, 1982.

Zhang, Q., Zheng, Y., Tong, D., Shao, M., Wang, S., Zhang, Y., Xu, X., Wang, J., He, H., Liu, W., Ding, Y., Lei, Y., Li, J., Wang, Z., Zhang, X., Wang, Y., Cheng, J., Liu, Y., Shi, Q., and Hao, J.: Drivers of improved $PM_{2.5}$ air quality in China from 2013 to 2017, P. Nat. Acad. Sci. USA, 116, 201907956, https://doi.org/10.1073/pnas.1907956116, 2019.

Zhang, W., Wang, H., Zhang, X., Peng, Y., Zhong, J., Wang, Y., and Zhao, Y.: Evaluating the contributions of changed meteorological conditions and emission to substantial reductions of $PM_{2.5}$ concentration from winter 2016 to 2017 in Central and Eastern China, Sci. Total Environ., 136892, https://doi.org/10.1016/j.scitotenv.2020.136892, 2020.

Zhang, W., Zhang, X., and Wang, H.: The role of aerosol-radiation interaction in the meteorology prediction at the weather scale in the numerical weather prediction model, Geophys. Res. Lett., 49, e2021GL097026, https://doi.org/10.1029/2021GL097026, 2022.

Zhang, X., Xu, X., Ding, Y., Liu, Y., Zhang, H., Wang, Y., and Zhong, J.: The impact of meteorological changes from 2013 to 2017 on $PM_{2.5}$ mass reduction in key regions in China, Sci. China Earth Sci., 62: 1885–1902, https://doi.org/10.1007/s11430-019-9343-3, 2019.

Zhang, Z., Xu, X., Qiao, L., Gong, D., Kim, S-J., Wang, Y., and Mao, R.: Numerical simulations of the effects of regional topography on haze pollution in Beijing, Sci. Rep., 8, 5504, https://doi.org/10.1038/s41598-018-23880-8, 2018.

Zhao, B., Liou, K.-N., Gu, Y., Li, Q., Jiang, J. H., Su, H., He, C. L., Tseng, H. L., Wang, S. X., Liu, R., Qi, L., Lee, W. L., and Hao, J. M.: Enhanced $PM_{2.5}$ pollution in China due to aerosol-cloud interactions, Sci. Rep., 7, 4453, https://doi.org/10.1038/s41598-017-04096-8, 2017.

Zheng, B., Tong, D., Li, M., Liu, F., Hong, C., Geng, G., Li, H., Li, X., Peng, L., Qi, J., Yan, L., Zhang, Y., Zhao, H., Zheng, Y., He, K., and Zhang, Q.: Trends in China's anthropogenic emissions since 2010 as the consequence of clean air actions, Atmos. Chem. Phys., 18, 14095–14111, https://doi.org/10.5194/acp-18-14095-2018, 2018.

Zheng, G. J., Duan, F. K., Su, H., Ma, Y. L., Cheng, Y., Zheng, B., Zhang, Q., Huang, T., Kimoto, T., Chang, D., Pöschl, U., Cheng, Y. F., and He, K. B.: Exploring the severe winter haze in Beijing: the impact of synoptic weather, regional transport and heterogeneous reactions, Atmos. Chem. Phys., 15, 2969–2983, https://doi.org/10.5194/acp-15-2969-2015, 2015.

Zhong, J., Zhang, X., Dong, Y., Wang, Y., Liu, C., Wang, J., Zhang, Y., and Che, H.: Feedback effects of boundary-layer meteorological factors on cumulative explosive growth of $PM_{2.5}$ during winter heavy pollution episodes in Beijing from 2013 to 2016, Atmos. Chem. Phys., 18, 247–258, https://doi.org/10.5194/acp-18-247-2018, 2018b.

Zhong, J., Zhang, X., Wang, Y., Liu, C., Dong, Y.: Heavy aerosol pollution episodes in winter Beijing enhanced by radiative cooling effects of aerosols, Atmos. Res., 209, 59–64, https://doi.org/10.1016/j.atmosres.2018.03.011, 2018a.

Zhong, J., Zhang, X., Wang, Y., Sun, J., Zhang, Y., Wang, J., Tan, K., Shen, X., Che, H., Zhang, L., Zhang, Z., Qi, X., Zhao, H., Ren, S., and Li, Y.: Relative contributions of boundary-layer meteorological factors to the explosive growth of $PM_{2.5}$ during the red-alert heavy pollution episodes in Beijing in December 2016, J. Meteorol. Res., 31, 809–819, https://doi.org/10.1007/s13351-017-7088-0, 2017.